Dr. 2345

310
2/3/81
T.S.

MASTER

N715-25
Bins-244

DOE/ET/15529-T1

FOSSIL ENERGY

MHD ELECTRODE DEVELOPMENT

Quarterly Report for Period April—June 30, 1980

By

John W. Sadler
Laurence H. Cadoff
Don L. Dietrick
James A. Dilmore
Edsel W. Frantti
Dave Jacobs
James R. Schornhorst
Edgar L. Kochka
Jack A. Kuszyk
S. K. Lau
Joseph Lempert
Jack C. Reck
Barry R. Rossing
Eugene E. Smeltzer

August 1980

Work Performed Under Contract No. AC01-79ET15529

Westinghouse Electric Corporation
Pittsburgh, Pennsylvania

U. S. DEPARTMENT OF ENERGY

DISTRIBUTION OF THIS DOCUMENT IS UNLIMITED

DISCLAIMER

This report was prepared as an account of work sponsored by an agency of the United States Government. Neither the United States Government nor any agency Thereof, nor any of their employees, makes any warranty, express or implied, or assumes any legal liability or responsibility for the accuracy, completeness, or usefulness of any information, apparatus, product, or process disclosed, or represents that its use would not infringe privately owned rights. Reference herein to any specific commercial product, process, or service by trade name, trademark, manufacturer, or otherwise does not necessarily constitute or imply its endorsement, recommendation, or favoring by the United States Government or any agency thereof. The views and opinions of authors expressed herein do not necessarily state or reflect those of the United States Government or any agency thereof.

DISCLAIMER

Portions of this document may be illegible in electronic image products. Images are produced from the best available original document.

DISCLAIMER

"This book was prepared as an account of work sponsored by an agency of the United States Government. Neither the United States Government nor any agency thereof, nor any of their employees, makes any warranty, express or implied, or assumes any legal liability or responsibility for the accuracy, completeness, or usefulness of any information, apparatus, product, or process disclosed, or represents that its use would not infringe privately owned rights. Reference herein to any specific commercial product, process, or service by trade name, trademark, manufacturer, or otherwise, does not necessarily constitute or imply its endorsement, recommendation, or favoring by the United States Government or any agency thereof. The views and opinions of authors expressed herein do not necessarily state or reflect those of the United States Government or any agency thereof."

This report has been reproduced directly from the best available copy.

Available from the National Technical Information Service, U. S. Department of Commerce, Springfield, Virginia 22161.

Price: Printed Copy A05
Microfiche A01

DOE/ET/15529-T1
Distribution Categories UC-90g and UC-93

MHD ELECTRODE DEVELOPMENT

Quarterly Report for the Period

April-June 30, 1980

John W. Sadler
Laurence H. Cadoff**
Don L. Dietrick
James A. Dilmore*
Edsel W. Frantti
Dave Jacobs
Edgar L. Kochka
Jack A. Kuszyk
S. K. Lau*
Joseph Lempert**
Jack C. Reck
Barry R. Rossing*
James R. Schornhorst
Eugene E. Smeltzer*

*Westinghouse Research & Development Center
**Consultant

WESTINGHOUSE ELECTRIC CORPORATION
Advanced Energy Systems Division
P. O. Box 10864
Pittsburgh, Pa. 15236

AUGUST 1980

PREPARED FOR THE
UNITED STATES DEPARTMENT OF ENERGY

Under Contract No. DE-AC-01-79-ET-15529

APPROVED:

John W. Sadler, Project Manager
Advanced Energy Systems Division

DISTRIBUTION OF THIS DOCUMENT IS UNLIMITED

TABLE OF CONTENTS

		Page
I.	ABSTRACT	1
II.	OBJECTIVE AND SCOPE OF WORK	2
	WBS 1.1 - ELECTRODE AND INSULATOR MATERIALS	3
	WBS 1.2 - ENGINEERING TESTS	3
	WBS 1.3 - WESTF MODIFICATION	6
	WBS 1.4 - PROJECT MANAGEMENT AND DOCUMENTATION	6
III.	SUMMARY OF PROGRESS TO DATE	7
	1.0 WBS 1.1 - ELECTRODE AND INSULATOR MATERIALS	7
	2.0 WBS 1.2 - ENGINEERING TESTS	10
	3.0 WBS 1.3 - WESTF MODIFICATION	13
	4.0 WBS 1.4 - PROJECT MANAGEMENT AND DOCUMENTATION	13
IV.	DETAILED DESCRIPTION OF TECHNICAL PROGRESS	14
	1.0 WBS 1.1 - ELECTRODE AND INSULATOR MATERIALS	14
	1.1 WBS 1.1.1 - Experimental Materials Fabrication	14
	1.1.1 Material Development	14
	1.1.2 Material Characterization	45
	1.2 WBS 1.1.2 - Laboratory Screening Tests	49
	1.2.1 Electrochemical Corrosion Tests	49
	1.2.2 Anode Arc Erosion Studies	49
	2.0 WBS 1.2 - ENGINEERING TESTS	57
	2.1 WBS 1.2.1 - Test Engineering	57
	2.1.1 Development Requirements	57
	2.1.2 Experiment Design	59
	2.1.3 Post-Test Analysis	62
	2.2 WBS 1.2.2 - Test Assembly Fabrication	67

TABLE OF CONTENTS (Continued)

		Page
	2.3 WBS 1.2.3 - WESTF Operations	76
	3.0 WBS 1.3 - WESTF MODIFICATIONS	76
	3.1 MINI-COMPUTER/DAS	76
	3.2 MAGNET INSTALLATION	76
	3.2.1 Magnet Modification	77
	3.2.2 General Modifications	81
	4.0 WBS 1.4 - PROJECT MANAGEMENT AND DOCUMENTATION	82
V.	SUMMARY PLANS NEXT REPORTING PERIOD	83
	WBS 1.1 - ELECTRODE AND INSULATOR MATERIALS	83
	WBS 1.2 - ENGINEERING TESTS	83
	WBS 1.3 - WESTF MODIFICATIONS	84
	WBS 1.4 - PROJECT MANAGEMENT AND DOCUMENTATION	84
VI.	CONCLUSIONS	85
VII.	REFERENCES	86

LIST OF TABLES

Table No.	Title	Page
1	Work Breakdown Structure	4
2	WESTF Test Capabilities	5
3	WESTF Test History	11
4	Platinum/Copper Interdiffusion at Different Hot Pressing Conditions	27
5	Electron Microprobe Interdiffusion Penetration Analysis after 5 Hours at 850°C, 1000 psi	37
6	Deposition Parameters, TiB_2 on Copper	39
7	Composition (w/o) of Arc-Tested Alloys	54
8	Calculated Slag Compositions from WESTF Test #43	64

LIST OF FIGURES

Figure No.	Title	Page
1	Program Schedule and Status	8
2	Metal Corrosion from Alkali - Sulfur Compounds	17
3	High Temperature Hot Corrosion of Various Superalloys	17
4	The Effect of Chromium on the Hot Resistance of Nickel Based Alloys	20
5	Cu-Pt Phase Diagram	25
6	Diffusion of Copper into Platinum at Different Test Conditions	29
7	Copper/Platinum Diffusion Bond Hot Pressed at 500°C for 5 Hours at 1000 psi in Argon	30
8	Schematic Concentration-Penetration Curve for a Semi-Infinite Diffusion Couple, Boltzmann-Matano Analysis	31
9	Predictive Extrapolation of Interdiffusion Zone Width	31
10	Platinum-Copper Interdiffusion Coefficients for Diffusion Bond at 850°C for 5 Hours	33
11	Interdiffusion Zone Between Copper and Four Refractory Metals	35
12	Specimen for Materials Test Section	38
13	Surface of TiB_2 Clad Copper Specimens from BCL	38
14	Scanning Electron Microscope Photograph of the Central Region of Sample 2	41
15	Scanning Electron Microscope Photograph of the Outer Ring of Sample 2	42
16	Photograph of a Cross Section of Sample 2	43
17	Attachment of 0.5 $SrZrO_3 \cdot 0.5\ (Sr_{.25}La_{.75}FeO_3)$ to Copper Mesh	46
18	Attachment of 30 m/o In_2O_3-20 m/o $PrO_{1.8}$-3.0 m/o Yb_2O_3-47 m/o HfO_2 to Copper Mesh	47
19	Thermal Conductivity Type MMM Ceramic	48
20	Schematic of New Anode-Arc Corrosion Test	50
21	The Effect of Arc, Corrodents and Surface Temperature on Corrosion of Copper	52
22	Anode-Arc Corrosion of Various Metal Materials	55

LIST OF FIGURES (Continued)

Figure No.	Title	Page
23	Steady State Temperature Distribution (°C) Copper Sample with 304 Stainless Steel Clad	58
24	Typical WESTF Test Section Frame	60
25	WESTF Test Section for WESTF Test 50	61
26	SEM Photomicrographs of Slag Layers on Cathode and Anode from Electrode #5, WESTF Test #43	63
27	SEM Photomicrograph of Grain Boundary Corrosion of Iron Cathode	66
28	SEM Photomicrograph of Slag Intruded Surface Region of ZrO_2 - 20 m/o Y_2O_3 Cathode - WESTF Test 45	68
29	Dummy Test Section Flow Train Components	70
30	WESTF II Prototype Frame Assembly	71
31	Key Components of WESTF II Peg Wall Assembly	72
32	Mechanical Testing of G-11 Frame	74
33	WESTF Status Photo	78
34	WESTF Status Photo	79

I. ABSTRACT

Technical progress under DOE Contract DE-AC-01-79-ET-15529 during the April to June 1980 quarter is presented.

Emphasis within this program is now being directed towards the engineering development of cold metallic electrodes, and in particular the identification and evaluation of alternatives to platinum for use as anodes. A literature search, concentrating on hot corrosion resistant alloys, has been undertaken and results are presented. In addition, results of platinum-copper diffusion studies and a preliminary evaluation of sputter coated specimens of TiB_2 clad copper are reported.

Laboratory anode arc erosion studies have continued. A number of modifications incorporated in the test setup are described. This modified test arrangement has been used to obtain comparative data on a number of potential anode metal alloys. Further work is required to refine the test, particularly to provide a reliable method of applying corrodent to the specimens under test. No significant laboratory electrochemical corrosion tests were completed during this reporting period.

Facility test operations were suspended upon completion of WESTF Test 49 during the prior quarter to permit basic facility modifications in support of the addition of a 3 Tesla magnet. The status of design, procurement and modification activities is presented.

II. OBJECTIVE AND SCOPE OF WORK

In continuation of the program to develop MHD power generation to commercial feasibility, Westinghouse is conducting a program to develop improved electrode designs for open-cycle coal-fired MHD generator applications. The program includes the link between basic and supportive materials development and testing in an engineering test rig that offers an adverse MHD environment for extended periods of time.

Specific development activities of this program are as follows:

(a) Laboratory screening tests to provide preliminary electrochemical stability data on selected advanced or modified ceramic candidate electrode and insulation materials.

(b) Laboratory screening tests to evaluate the resistance of selected candidate anode materials to simulated arc impingements under a representative range of chemical and thermal conditions.

(c) Engineering rig tests of preferred electrode designs, selected on the basis of the screening test results and/or pertinent outside data, under simulated open-cycle coal-fired MHD operating conditions.

(d) Preparation and fabrication of experimental electrode materials, as warranted by favorable laboratory screening test results, to provide samples for engineering rig tests.

In addition to these four main development activities, this project includes providing such laboratory, design, test and analytical support as necessary to characterize test materials, and to determine such essential physical and chemical properties as are required to properly design the test specimens and to interpret and analyze test data. Dependent on development results, preferred electrode materials will be prepared for advanced testing in other DOE contractor facilities.

These objectives are being pursued in accordance with a statement of work which is consistent with the National Plan for MHD development formulated by DOE.

The major elements of the program are presented in a Work Breakdown Structure which is presented in Table 1. The Level I effort is the MHD Electrode Development Contract, and Level II consists of the following four tasks.

WBS 1.1 ELECTRODE AND INSULATOR MATERIALS
WBS 1.2 ENGINEERING TESTS
WBS 1.3 WESTF MODIFICATION
WBS 1.4 PROJECT MANAGEMENT AND DOCUMENTATION

WBS 1.1 - ELECTRODE AND INSULATOR MATERIALS

The objective of this task is to provide for the development, laboratory evaluation and fabrication of electrode and insulator materials. All necessary experimental material preparation, as well as fabrication of test samples for laboratory screening tests, engineering rig tests in the Westinghouse Electrode System Test Facility, WESTF (WBS 1.2), or other tests will be completed under this task. This task also includes supporting pre-test material characterization and laboratory screening tests used to evaluate the relative performance of candidate materials. These screening tests include electrochemical and anode arc impingement tests.

WBS 1.2 - ENGINEERING TESTS

The objective of this task is to provide for the engineering tests of promising electrode/insulator materials resulting from the WBS 1.1 activity. In particular, this task provides for the supporting design, test and post-test analysis effort as well as maintenance and operation of the engineering test rig, WESTF. Table 2 summarizes WESTF test capabilities.

This task incorporates the elements of planning, experiment design, test operations and post-test analysis and provides the close engineering design and test discipline necessary to effect successful electrode/insulating wall system development. In addition, final fabrication and assembly operations necessary to incorporate electrode and interelectrode insulating elements fabricated under WBS 1.1 into a complete assembly ready for testing in WESTF

TABLE 1

WORK BREAKDOWN STRUCTURE

(SUBELEMENTS TO DOE WBS 2.2.2)

WBS 1.0 MHD ELECTRODE DEVELOPMENT

- WBS 1.1 ELECTRODE AND INSULATOR MATERIALS
  - WBS 1.1.1 EXPERIMENTAL MATERIALS FABRICATION
    - MATERIAL DEVELOPMENT
    - MATERIAL CHARACTERIZATION
    - MATERIAL FABRICATION
  - WBS 1.1.2 LABORATORY SCREENING TESTS
    - ELECTROCHEMICAL TESTS
    - ANODE ARC TESTS
- WBS 1.2 ENGINEERING TESTS
  - WBS 1.2.1 TEST ENGINEERING
    - DEVELOPMENT REQUIREMENTS
    - EXPERIMENT DESIGN
    - POST-TEST ANALYSIS
  - WBS 1.2.2 TEST ASSEMBLY FABRICATION
  - WBS 1.2.3 WESTF OPERATIONS
    - PRE-TEST ACTIVITY
    - TEST OPERATIONS
- WBS 1.3 WESTF MODIFICATION
- WBS 1.4 PROJECT MANAGEMENT AND DOCUMENTATION

I II III - SYSTEMS LEVEL

TABLE 2

WESTF TEST CAPABILITIES

Mass Flow	To 0.5 lb/sec
Combustion Temperature	To $2850^{o}K$
Combustor Pressure	1 to 5 atm
Channel Velocity	Subsonic, 500 to 800 m/sec
Seeding	K_2CO_3 or K_2SO_4 wet with ash or char additions (Rosebud)
B Field	3 Tesla, nominal - 3.3 Tesla, objective
Fuel	Toluene/#2 Fuel Oil
Oxidant	Preheated air with oxygen enrichment
Data Collection	240 channels coupled with minicomputer
Test Duration	Up to 100 hours
Test Frequency	Up to 2 per month
Channel Configuration	12.5 cm^2 flow cross section
Startup Ramp, Minimum	$\approx 25^{o}K/min$

will be provided under this task. Required test documentation and facility operating procedures will also be prepared.

WBS 1.3 - WESTF MODIFICATION

This task has been established to provide for the planned modification of WESTF. The primary element of this task is the addition of a conventional 3.0 tesla magnet.

WBS 1.4 - PROJECT MANAGEMENT AND DOCUMENTATION

This centralized management task provides the focal point for directing the activities which comprise the full project effort. The Project Manager is responsible for the proper definition, integration and implementation of the technical, schedule, contractual, and financial aspects of the program. Coordination of the preparation of required documentation will also be completed under this task.

III. SUMMARY OF PROGRESS TO DATE

During the April to June 1980 quarter, the principal areas of activity were as follows:

- Continuation of electrode material development activities with emphasis on identifying alternative materials to replace platinum as an anode clad material.
- Continuation of laboratory anode arc testing with emphasis on improving the general test methodology and reliability.
- Completion of the design of the cold metallic electrode WESTF Test Section for use with the magnet (WESTF II).
- Completion of magnet modification activities.
- Continuation of WESTF modifications as required to support installation of the magnet.
- Initiation of fabrication of the initial WESTF II Test Section.

Figure 1 summarizes the overall program schedule, based on the approved Project Management Summary Baseline Report, FY 80 Revision dated October 1979, and shows schedular status. Throughout this quarter WESTF has been shut down and modifications associated with magnet installation are in progress.

1.0 WBS 1.1 - ELECTRODE AND INSULATOR MATERIALS

In addition to providing necessary test materials, for the laboratory screening tests and WESTF tests, and material characterization data required for the detail design activity, this task includes a number of electrode and insulator materials development and evaluation activities.

A number of candidate insulator materials have been evaluated on the basis of corrosion resistance in Western coal slag. On the basis of this immersion test (Reference 1), the following materials have been ranked as excellent:

DOE Form CR-635 (1-78)

U.S. DEPARTMENT OF ENERGY

MILESTONE SCHEDULE AND STATUS REPORT

1. Contract Identification: MHD ELECTRODE DEVELOPMENT PROGRAM	2. Reporting Period: through 3/80	3. Contract Number: DE-AC-01-79-ET-15529
4. Contractor (name, address): WESTINGHOUSE ELECTRIC CORPORATION ADVANCED ENERGY SYSTEMS DIVISION P. O. Box 10864 Pittsburgh, Pa. 15236		5. Contract Start Date: April 23, 1979 6. Contract Completion Date: September 30, 1980

7. Identification Number WBS	8. Reporting Category (e.g., contract line item or work breakdown structure element)	9. Fiscal Years and Months: 79 1Q, 2Q, 3Q, 4Q; 80 O, N, D, J, F, M, A, M, J, J, A, S	10. Percent Complete a) Planned	b) Actual
1.1	ELECTRODE AND INSULATOR MATERIALS			
1.1.1	EXPERIMENTAL MATERIALS FABRICATION			
1.1.2	LABORATORY SCREENING TESTS			
1.2	ENGINEERING TESTS			
1.2.1	TEST ENGINEERING			
1.2.2	TEST ASSEMBLY FABRICATION			
1.2.3	WESTF OPERATIONS			
1.3	WESTF MODIFICATION			
1.4	PROJECT MANAGEMENT AND DOCUMENTATION			

11. Remarks

12. Signature of Contractor's Project Manager and Date: John W. Sadler	13. Signature of Government Technical Representative and Date

Figure 1. Program Schedule and Status

Al_2O_3	Fused Cast	Carborundum
Al_2O_3-Cr_2O_3	Fused Cast	Carborundum
$MgAl_2O_4$-Cr_2O_3	Fused Cast	Carborundum
$MgAl_2O_4$	Fused Cast	Carborundum
$MgAl_2O_4$	Fused Cast	Trans-Tech
MgO	Fused Cast	Norton

Laboratory electrochemical corrosion tests and anode arc erosion tests have been conducted to evaluate the relative performance of candidate electrode materials. The following summarizes significant findings in these areas:

- A comprehensive model for understanding electrochemical reactions in slagging MHD channels has been developed (Reference 1).
- Zirconia based materials appear to be extremely promising candidate materials for use as anodes with Western slags under slagging hot and perhaps non-slagging super-hot conditions (Reference 2).
- Electrochemical corrosion is extremely sensitive to density and purity of electrode materials (Reference 2).
- Iron cathodes and platinum anodes form the most promising metal electrode combination identified to date for use under slagging hot conditions.
- Slag chemistry modification, through additions of transition metal ions, is effective in minimizing electrochemical corrosion and polarization (Reference 3).
- Laboratory scale anode arc tests indicate that TiB_2 coated copper may be comparable to platinum clad copper in the slagging cold operating mode (Reference 4).

As reported in Section IV - 1.1.1, the MHD channel environment at the anode is similar to that encountered in gas turbine and fireside coal atmospheres. The subject of hot corrosion resistant alloys has been searched to aid in identifying those materials which are the most promising alloys to replace platinum as an anode cladding material. Preliminary results of this literature search are presented. In addition, this section presents results of platinum-copper diffusion studies as well as an evaluation of sputter coated specimens of TiB_2 clad copper prepared by Battelle Columbus Laboratories (BCL).

Continuing results from the laboratory anode arc tests are presented in Section IV - 1.2.2. In addition a number of improvements incorporated in the test setup are discussed, as well as further improvements in test methodology required to enhance the reliability of this laboratory screening test.

2.0 WBS 1.2 - ENGINEERING TESTS

This task is directed towards the design, fabrication, test and post-test analysis of those electrode/insulator materials which undergo testing in the Westinghouse Electrode System Test Facility (WESTF). In comparison with laboratory screening tests, which generally couple only one or two aspects of the MHD channel environment, WESTF provides a realistic simulation of the MHD channel environment. Inclusion of magnetic field effects is planned, see WBS 1.3 below.

Table 3 provides a summary of WESTF tests completed to date. Implicit in this test summary are the following accomplishments:

- Satisfactory operation of WESTF: in the clean firing super-hot mode; in the slagging cold mode with Eastern and Western slags; in the slagging hot mode with Western slag.
- WESTF Tests 40 and 41, slagging cold electrodes, have established a correlation with laboratory and generator tests.
- Testing of electrodes and electrode materials supplied by others, including: AVCO, BPNL, and MIT.

TABLE 3

WESTF TEST HISTORY

OPERATING MODE	CLEAN	CLEAN COLD	CLEAN SH	CLEAN SH	CLEAN SH	CLEAN SH	SLAG COLD
Test ID	D-7	W-35	W-36	W-37(2)	W-38(2)	W-39(2)	D-8
Test Section	Dummy	WESTF	WESTF	WESTF	WESTF	WESTF	Dummy
Approx. Date	5/77-6/77	7/77-9/77	9/77	10/77	11/77	1/78	6/78-9/78
Electrode Material(1)	NA	Cu	$LaCrO_3$	MAFF 31 MAFF 41 HfO_2 Comp.	$LaCrO_3$(3) $LaCrO_3ZrO_2$ $LaCrO_3$	$LaCrO_3$-$LaAlO_3$ $LaCrO_3$-$SrZrO_3$ $LaCrO_3$ MAFF 31	NA
Insulator Material	NA	$MgAl_2O_4$	$MgAl_2O_4$ MgO	$MgAl_2O_4$	$MgAl_2O_4$ MgO	$MgAl_2O_4$ MgO	NA
T_E, °C.	NA	400-100	1700	1700+	1700+	1700+	NA
J, amp/cm^2	NA	To 1.0	1.0	1.0	1.0	1.0	NA
Q, w/cm^2	NA	~90	~30	~30	~30	~30	NA
B, Tesla	NA	NA	NA	NA	NA	NA	NA
Axial Field, Kv/m	NA	No	No	No	No	No	NA
Ash Type	NA	NA	NA	NA	NA	NA	Rosebud
Seed	K_2CO_3	K_2CO_3	K_2CO_3	K_2CO_3	K_2CO_3	K_2CO_3	K_2CO_3
SO_2 Level, m/o	--	--	--	--	--	--	--
Duration-Hrs.	NA	22	20	20	20	20	NA

OPERATING MODE	SLAG COLD	SLAG COLD	NON-SLAG SH	NON-SLAG SH	CLEAN SH	NON-SLAG SH	SLAG COLD
Test ID	W-40	W-41	D-9	D-10	D-11	45	47
Test Section	WESTF	WESTF	MTS(6)	Transition	Transition	MTS	MTS II
Approx. Date	10/78-1/79	1/79-8/79	9/79	10/79	11/79	12/79	1/80
Electrode Material(1)	Cu	Cu-Pt (+) Cu-W/Cu (-)	$LaCrO_3$	NA	NA	Zirconia	Cu-Pt (+) Cu (-)
Insulator Material	$MgAl_2O_4$	BN	MgO	MgO	MgO	NA	MgO
T_E, °C	150/275	150	To 1900	NA	NA	1800	150
J, amp/cm^2	To 1.25	0.9	NA	NA	NA	0.9	1.0
Q, w/cm^2	~125	~125	--	NA	NA	30	~125
B, Tesla	NA	NA	NA	NA	NA	NA	NA
Axial Field, Kv/m	Yes	Yes	No	No	No	No	No
Ash Type	Eastern	Eastern	Rosebud	Rosebud	--	Rosebud	Rosebud
Seed	K_2CO_3	K_2CO_3	K_2CO_3	K_2CO_3	K_2CO_3	K_2CO_3	K_2CO_3
SO_2 Level, m/o	0.01	0.01	0.01	0.01	0.01	0.06	0.3
Duration-Hrs.	14(4)	63(5)	5(7)	13(5)	11	9	7

(1) Anode and Cathode Unless Otherwise noted
(2) U-02 Phase III Proof Test
(3) With ZrO_2
(4) Four Runs
(5) Two Runs
(6) Materials Test section
(8) BPNL Material
(9) MIT Material

TABLE 3

WESTF TEST HISTORY (Continued)

OPERATING MODE	NON-SLAG SH	SLAG HOT	NON-SLAG SH				
Test ID	42	43	49				
Test Section	WESTF	WESTF	WESTF				
Approx. Date	1/80	3/80	3/80				
Electrode Material[1]	Hafnia Based[8] Zirconia Based	Pt (+) Fe (-)	$LaFeO_3$, $SrZrO_3$, $SrFeO_3$[9]				
Insulator Material	NA	$MgAl_2O_4$ Al_2O_3	MgO				
T_E, °C	1250 to 1750	1050-1400	1700				
J, amp/cm^2	0	1.0	1.0				
Q, w/cm^2	15 to 30	60-115	40				
B, Tesla	NA	NA	NA				
Axial Field, Kv/m	No	No	No				
Ash Type	Rosebud	Rosebud	Rosebud				
Seed	K_2CO_3	K_2CO_3	K_2CO_3				
SO_2 Level, m/o	0.06	0.06	0.06				
Duration-Hrs.	22	13	8				

As presented in Section IV-2.1.2, detail design of the WESTF Test Section for slagging cold metallic systems has been completed. Section IV-2.1.3 presents the results of WESTF Test 43 post-test analysis efforts completed this quarter. Fabrication activities are discussed in Section IV-2.2.

As previously reported, WESTF test operations were suspended at the close of the prior quarter to permit facility modification as required by the addition of a conventional 3 Tesla magnet. The total WESTF operating time, defined as the cumulative time interval from combustor on to combustor off, is unchanged at 438 hours. Of this total time, 198 hours were accumulated under clean firing conditions and 240 hours were accumulated under slagging conditions.

3.0 WBS 1.3 - WESTF MODIFICATION

Activity within this task is directed towards extending the capabilities of WESTF and incorporating facility and operational improvements. The major activity is that associated with the addition of a conventional 3 Tesla magnet.

At the completion of WESTF Test 49 in mid-March, the facility was shut down for those modifications required by the magnet addition. Extensive rework of the facility is in progress.

In this regard, the magnet modification has been completed and the unit has been delivered to and positioned in Building 301 of the R&D Center. As also presented in Section IV-3.0 plugging of the coil coolant channels greatly extended the time for completion of the magnet modifications and impacted other facility modification activities.

4.0 WBS 1.4 - PROJECT MANAGEMENT AND DOCUMENTATION

Significant project documentation issued during this quarter included the following:

- Quarterly Report, January-March 1980.
- Monthly Project Management Reports

IV. DETAILED DESCRIPTION OF TECHNICAL PROGRESS

Program activities have been redirected to provide emphasis on the engineering development and evaluation of slagging cold metallic electrodes, and in particular on identifying alternatives to platinum as a cladding for anode electrodes. As a result a number of activities are in a period of transition. A work plan is being formulated to reflect the change in program emphasis. This work plan will reflect the results of a literature search which has been directed at identifying alloys for use as slagging cold metallic anodes. Preliminary results of this literature search are presented in the following section.

1.0 WBS 1.1 - ELECTRODE AND INSULATOR MATERIALS

1.1 WBS 1.1.1 - Experimental Materials Fabrication

1.1.1 Material Development

Electrode Materials

Alloy Selection for Cold Metallic Anodes

It is important to identify economic alternative materials to platinum, as an anode clad material, that will sustain long term open-cycle, coal-fired MHD generator operations. To accomplish this one must first examine the conditions that exist at the anode wall and then establish criteria for selecting potential materials.

The MHD channel environment is relatively reducing (Reference 5) and as a first guess one would tend to select materials which are resistant to a high sulfur, low oxygen pressure environment (i.e. coal gasification atmospheres). However, it is now well established by laboratory and channel tests (References 3,6,7 and 8) that highly oxidizing environments are electrochemically generated at the anode. This is a result of anion migration (O^{-2} and probably SO_2^{-2}) through the electrolytic slag layer under a voltage gradient to the anode where discharge reactions occur (i.e. O_2, SO_3). Arcs can only expedite this process. They create a plasma due

to vaporization and ionization of slag components allowing anions to be driven towards the anode. Arcs also create a liquid pool in the slag layer wherein O^{-2} and SO_4^{-2} anions are electrically transferred to the anode. Although the atmosphere at the anode is not quantitatively known, it is probable that it is a highly oxidizing O_2 and SO_3 rich environment akin to that which occurs when coal is burned in an oxygen rich atmosphere, i.e. a hot corrosion atmosphere. This is similar to gas turbine and fireside coal atmospheres. Thus, in selecting a potential corrosion resistant anode alloy, we can draw on the available information on the subject of hot corrosion resistant alloys (References 9 to 21).

In addition to hot corrosion resistance, the other major requirement is that the anode material be resistant to arc erosion. Arcs, which punch their way through the slag layers into the anode alloy, can cause high metal wastage by vaporization, melting, thermal shock of the protective scale, and by thermally enhanced chemical/electrochemical reactions. Although there is little experimental work detailing arc attack mechanisms, it is clear that anode alloy selection criteria should be based on its being refractory and on its having a refractory protective scale. The scale should in turn have high thermal and electrical conductivity, high thermal shock resistance and high resistance to being fluxed by molten slag.

In the next sections we will review the important factors affecting the ability of alloys to resist anodic corrosion/erosion. This is based on a search of the literature on hot corrosion.

Hot Corrosion

With the exception of some noble metals such as platinum, most metal alloys designed for oxidation-hot corrosion resistance depend on the formation of protective Cr_2O_3 or Al_2O_3 scales*. If adherent and defect free, these scales inhibit the motion of cations out to the atmosphere/oxide interface and O^{-2} or SO_4^{-2} anion movement to the metal interface, thereby insulating the alloy from further attack. In addition to the chromium and/or aluminum components, corrosion resistant alloys are comprised of the base elements Fe and/or Ni and/or Co and also contain solid solution strengthening elements such as Mo, W, Nb and Ta and Ti, Nb, Ta precipitate and carbide formers. Generally, most

*In most alloys, other scales (base metal oxides, spinels) are also formed but only Al_2O_3 and Cr_2O_3 are truly protective.

alloys need more than 15 w/o Cr and less than 5 w/o Al to form a continuous Cr_2O_3 scale. Alloys with more than 5 w/o Al tend to form Al_2O_3 coatings. Al_2O_3 scale forming alloys' resistance to corrosion improves as the Cr content increases. In severe hot corrosion environments, the best alloys should contain more than 5 w/o Cr for Cr_2O_3 scale forming alloys and more than 8% Al for Al_2O_3 scale forming alloys.

Hot corrosion is a form of accelerated oxidation, the accelerating agent usually being a liquid phase which deposits on the alloy from the combustion atmosphere. In coal fired systems, the liquid corrodents are normally compounds of alkali metals (K, Na) and sulfur. The temperature ranges where accelerated corrosion occurs are related to the melting points of these various sulfur compounds. Thus, in many cases, the corrosion rate as a function of temperature exhibits a bell shaped curve dependence as shown in Figure 2. In these bell curves, the onset or threshold corrosion temperature corresponds to the melting point of the corrodent (or corrodent - alloy reaction products), the peak corrosion temperature represents a maximum in diffusion controlled attack while the minimum or terminal corrosion temperature occurs near the dew point for the corrodents (or liquid reaction products). In the temperature range of ≈600-950°F, corrosion has been attributed to the formation of molten pyrosulfates $(Na, K)_2 S_2O_7$, while at the higher temperatures, ≈1100-1300°F, alkali trisulfates such as $(Na, K)_3 Fe (SO_4)_3$ are responsible for corrosion. Formation of both of these compounds requires high SO_3 partial pressures.

At the highest temperatures (≈1500-1950°F)*, hot corrosion reactions, which are often experienced by gas turbine alloys and which will probably be the dominant corrosion attack of MHD anode materials, results from the deposition of molten alkali sulfates. Bell shaped corrosion curves are often found for this type of corrosion as well. See for example Figure 3 which shows test results for various superalloys in residual oil fired conditions (no potassium) and for simulated clean MHD (K_2SO_4) conditions (Reference 8). High temperature hot corrosion is generally characterized by an incubation period (Reference 11 and 15) lasting

*Exact temperatures depend on the composition of the alloy and gas phases, i.e. Na:K ratio, SO_3 pressures, etc.

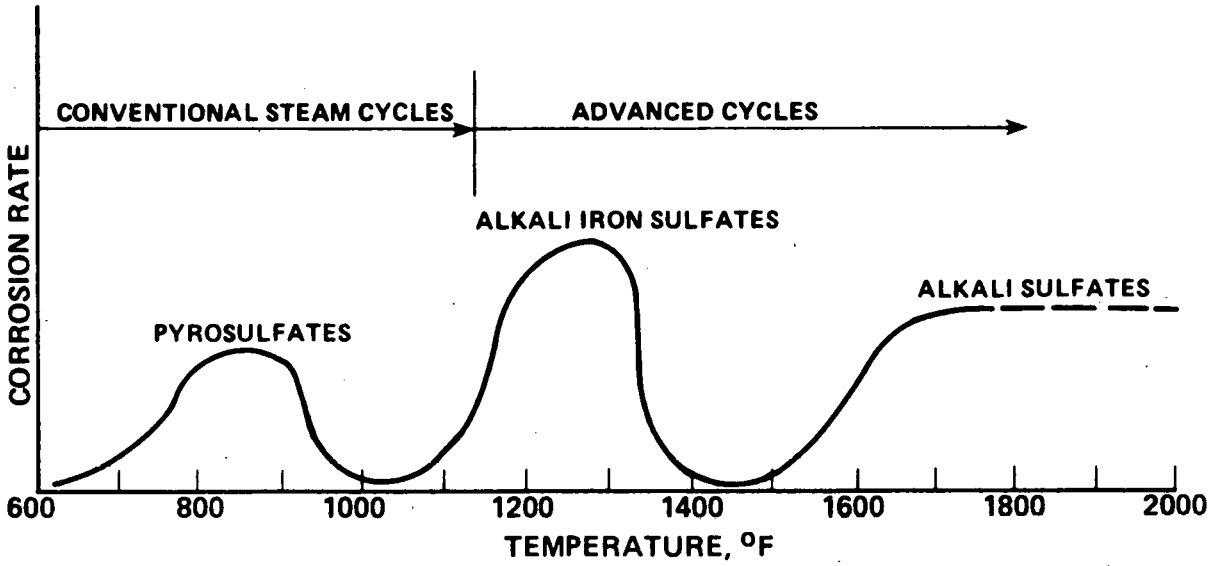

Figure 2. Metal Corrosion from Alkali - Sulfur Compounds (Reference 20)

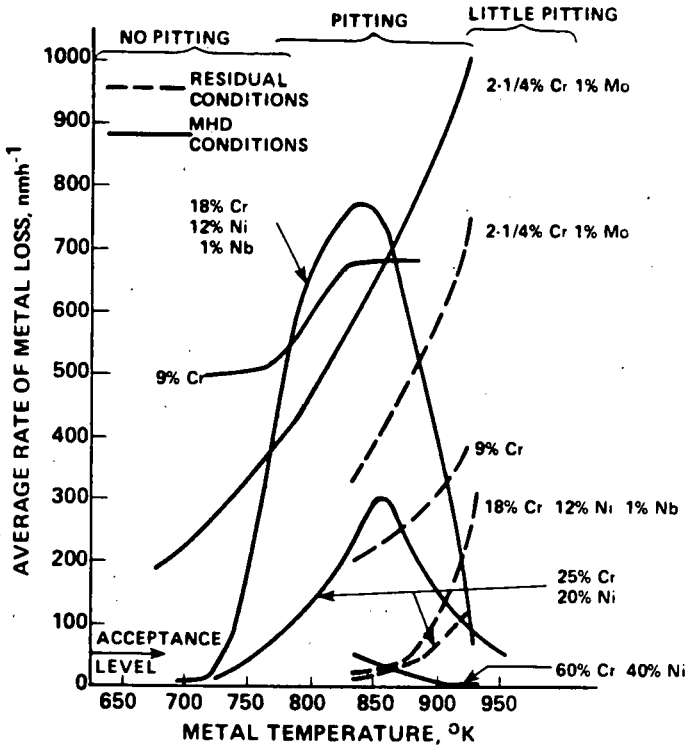

Figure 3. High Temperature Hot Corrosion of Various Superalloys. (70 Hour Test under Residual Oil Fired Conditions (no K) and clean MHD (K_2SO_4) Conditions) (Reference 8)

in some cases thousands of hours during which the oxidation of the alloy under the sulfate (i.e., K_2O_4) is the same or less than that in the absence of the salt. Stringer and Whittle (Reference 21) have shown that the initiation stage of hot corrosion involves the breakdown of the protective oxide layer, and once this occurs, corrosion attack propagates rapidly into the alloy. The scale breakdown may occur by mechanical processes brought about by thermal cycling or strain or physical erosion or by chemical processes such as scale fluxing by molten reactants or reactant induced loss of scale/metal adhesion.

It is generally acknowledged that there may be three major mechanisms for the propagation of hot corrosion:

(1) "basic fluxing" which involves degradation of a protective oxide scale by reaction with oxide ions from the dissociation of the alkali sulfate. This mechanism is predomient in O_2 rich, S deficient atmospheres;

(2) "acidic fluxing" where the oxide scale is degraded by the donation of oxide ions to the alkali sulfate, which occurs under high local SO_3 pressures; the presence of W, Mo, V etc., tends to accelerate this mode of attack, and

(3) "sulfidation" which involves the formation of sulfide in the alloy underneath the scale and the subsequent rapid preferential oxidation of these sulfides. The sulfidation reactions often locally depletes the concentration of those elements needed to form protective oxides thereby exposing the alloy to further attack.

Evidence for all of the above mechanisms has been found, but it is clear that alloy composition and the nature of the corrosive atmosphere determines which process actually dominates.

There is often conflicting data in the literature on corrosion mechanisms, rates and the role of alloy additives. This could be due to the fact that different test conditions were used in these experiments including laboratory immersion tests, gas turbine test rigs, potentiostatic measurements etc. Despite these conflicts, certain general patterns emerge and will be summarized below. Although

there are very few studies done under the slagging, high K, high S conditions remotely characteristic of MHD generators (Reference 3,6 and 10), the available data is not inconsistent with the following generalizations.

1) The presence of liquid phases (whether deposited from the atmosphere and/or reaction products themselves) are deleterious to hot corrosion resistance. Careful control over suface temperatures and/or gas chemistry are often used to minimize exposure to liquid phases.

2) The chromium content of an alloy is a critical factor in imparting corrosion resistance to an alloy. This is illustrated in Figure 4 for Ni based alloys.

3) Al_2O_3 tends to grow at a slower rate and forms a more protective scale than Cr_2O_3. However, Al_2O_3 is more likely to spall with thermal cycling. Alloy additions of 1 w/o La or Ce or Y or Hf are effective in minimizing spalling.

4) Cobalt based superalloys are generally considered to have superior hot corrosion resistance than nickel based alloys. This may reflect the fact that Co alloys often contain a higher Cr content. Little is known about the comparative hot corrosion behavior of Ni vis-a-vis Fe based alloys. There is some evidence that Ni alloys may be superior under oxidizing conditions (iron tends to form trisulfates) and somewhat inferior under reducing atmospheres (the Fe-FeS eutectic temperature is higher than Ni-NiS).

5) Elements such as Ta, Mo, W, Nb which are added to alloys to improve high temperature strength, via solid solutions or precipitation hardening mechanisms, are usually deleterious to hot corrosion resistance. It has been suggested that these elements accelerate corrosion by an acidic fluxing mechanism.

6) Alloying elements such as Cr, Al, Hf, Pt etc. which promote scale healing and/or adhesion will improve hot corrosion resistance. In particularly severe atmospheres, Cr_2O_3 scale alloys should contain at least 25-30 w/o Cr to insure growth

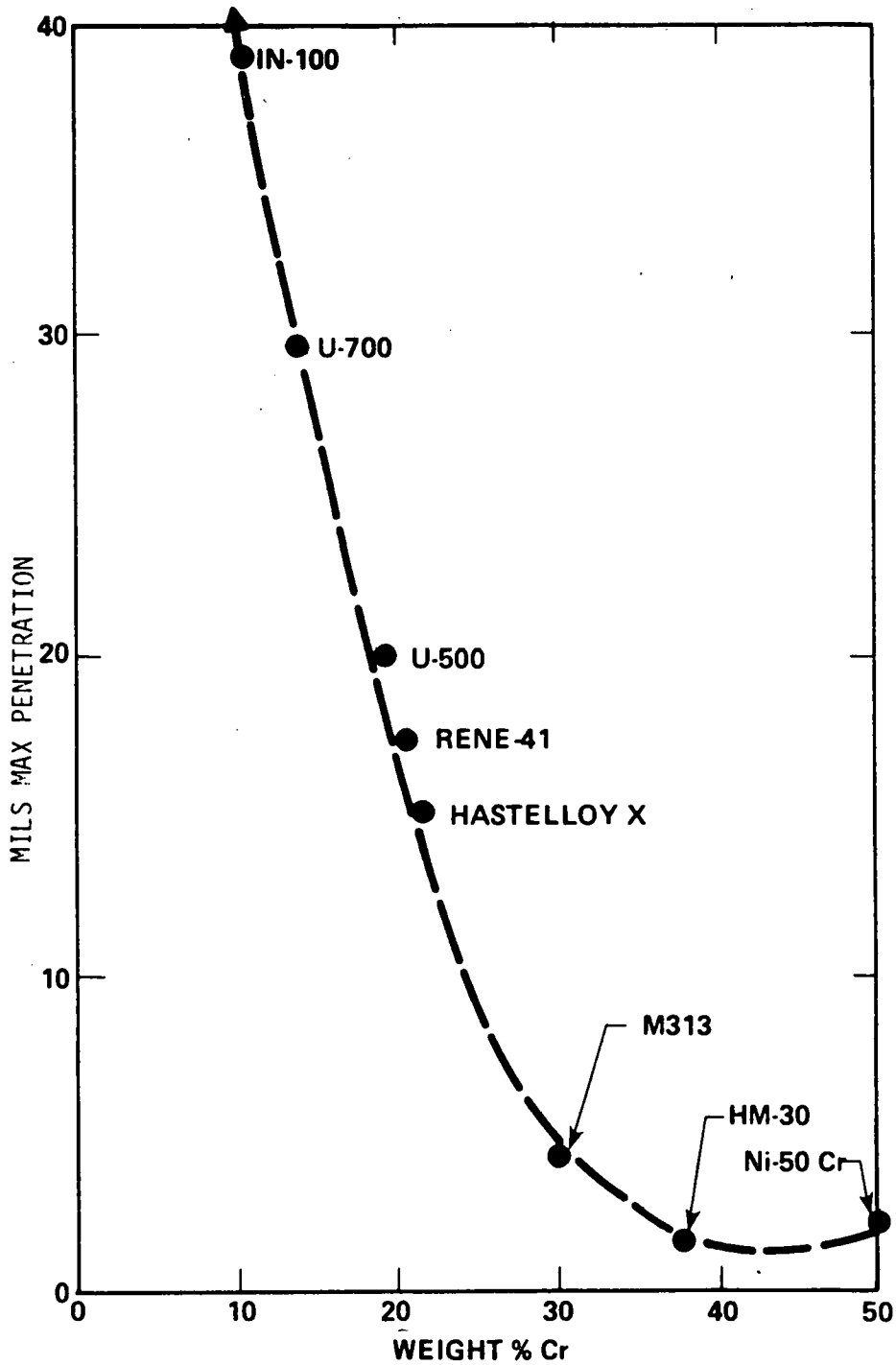

Figure 4. The Effect of Chromium on the Hot Corrosion Resistance of Nickel Based Alloys

and complete coverage of the alloy surface by the protective scale. Even in Al_2O_3 scale forming alloys, Cr contents should be more than 25 w/o and Al above 8 w/o. Platinum additions in quantities of about 5-10 w/o have been shown to be especially effective in improving hot corrosion resistance of Al_2O_3 scale forming alloys and Cr_2O_3 scale forming alloys with low Cr contents (Reference 22).

7) The combination of chloride (present especially in mid-western USA coals) and sulfate is far more corrosive than sulfate alone. Chlorine is believed to have a role in promoting scale rupture and in reducing scale/metal adhesion.

8) Potassium, in combination with sodium, is more aggressive than sodium alone. Also, corrosion increases with increasing potassium in the deposits. Relative corrosion resistance ranking of materials against Na alone, however, is the same as in tests with Na and K combined.

9) Alloys which have been pre-oxidized in sulfur free oxidizing atmospheres are subsequently more resistant to corrosion than if they had been directly exposed to sulfur containing hot corrosion atmospheres. It is believed that sulfur contributes to the formation of scales with high concentrations of defects, thereby promoting greater interdiffusion rates between corrodent and alloy species.

10) Coatings such as CoCrAlY, FeCrAlY and NiCrAlY have been shown to be effective in protecting alloys in aggressive atmospheres. Our studies (Reference 7) have suggested that TiB_2 may be as protective as Pt under simulated arc conditions using a western coal ash corrodent.

Arc Erosion

If the requirement for long lived MHD cold wall anodes was solely that of minimizing hot corrosion attack it would be a relatively simple problem to solve. First, it would be necessary to operate the anodes at temperatures where the corrodents were not liquid. Second, it would be necessary to select

alloys with inherently good hot corrosion resistance. Since the strength requirement of the electrode is low, simple binary or tertiary Cr_2O_3 or Al_2O_3 scale forming Co, Fe or Ni based alloys would be adequate.

However, conditions are more complex since the anode is an electrically active component of the MHD channel. It must be able to transfer current which is being carried by "arc columns" from the overlying slag layer to an exterior load. Intense localized heating will occur around the arc column as it impinges on the surface of the electrode and its protective scale. Excessive loss of material, which we will call "arc erosion", can occur due to vaporization, melting, thermal shock and spalling of protective coatings, and enhanced chemical and electrochemical (especially liquid phase) reactions. Too little is known about arc erosion to establish which of the above mechanisms dominates. In the following discussion we will speculate on some of the important thermal and electrical aspects of arc erosion.

The erosion of various materials by arcs is very dependent upon the local temperatures near the arc root. This temperature is dependent in turn upon the amount of energy in the arc, the residence time of the arc and material properties. The time required to bring a localized anode area under an anode arc spot of constant power to a given temperature is proportional to $K \rho C_p$ where K is the anode thermal conductivity, ρ is the anode density and C_p is the anode specific heat. Since the usual MHD arcs are mobile, the factor $K \rho C_p$ can be considered a figure of merit.

If $K \rho C_p$ is large enough, and the arc dwell time short enough, little or no arc erosion will be experienced. To minimize temperature excursions, it would be desirable to coat thin films of the alloys onto a high $K\rho C_p$ material such as copper. This may not be practical however due to the probability that the arc can blast a hole in the thin coating, thereby exposing the copper to catastrophic attack. All potential Co, Fe or Ni based alloys have approximately the same value of $K\rho C_p$ and no distinction can be made on that basis. Neither can distinctions be made on the preferability of using Al_2O_3 vis-a-vis Cr_2O_3 scale forming alloys. A copper base offers a distinct thermal advantage.

Another thermal criteria resulting from arc impingement must deal with the resistance of the scale to thermal shock, since rupture of the scale would expose the underlying alloy to rapid attack. The thermal shock resistance parameter is $R = \sigma / E\alpha$ where σ is the rupture strength, E is the elastic modulus and α is the coefficient of thermal expansion. The R factor for Al_2O_3 and Cr_2O_3 are nearly the same, so by this criteria both types of scale forming alloys are about equivalent. However, to insure rapid healing of a damaged coating, it is desirable that the Cr content be higher than 25 w/o. Pt additions at the 5-10 w/o levels have also been shown to be effective in increasing diffusion rates which should expedite scale healing (Reference 22).

The ability of an alloy to resist liquid phase attack (in the MHD case liquid alkali rich coal slag which has been melted by the arc) is critical to long term survival of anode alloys. Laboratory immersion tests at Westinghouse have shown the importance of high ceramic density in resisting slag attack. Fortunately our results have shown that under oxidizing conditions, Cr_2O_3 and Al_2O_3 are some of the most inert ceramics to liquid slag corrosion.

The electrical properties of the scale forming on the alloy should also be an extremely important factor in selecting alloys for arc erosion resistance. If the electrical resistivity is high the arc will be forced to blast through the scale (causing melting, vaporization, cracking) until it reaches the underlying alloy. The lower the electrical resistivity, the more diffuse the arc will be and in the extreme case where the conductivity of the scale approaches that of the metal, the damage can be quite small. Since the electrical conductivity of Cr_2O_3 is $\approx 10^7$ times greater than of Al_2O_3, it is reasoned that Cr_2O_3 scale forming alloys may perform better than Al_2O_3 forming alloys. However, the fact that for the same oxidizing conditions, Al_2O_3 scales are thinner than Cr_2O_3 scales may narrow the gap between selection of these two types of alloys.

In summary, the resistance of a material to anode arc erosion will clearly be a function of the energy and duration of the arc and the nature of the alloys and their protective scales. Of the potential Co, Fe or Ni based superalloys considered for hot corrosion resistance, it is likely that on most accounts, their arc erosion resistance will be about the same. The major point of departure

between alloys lies in the electrical conductivities of their scales and from this point of view, Cr_2O_3 scale forming alloys are probably superior to Al_2O_3 scale forming alloys. A list of specific recommendations for commercial alloys which offer potential for use as cold wall anodes is being prepared.

Platinum/Copper Diffusion

The current baseline anode material for slagging cold wall electrodes is platinum clad copper. Recent preliminary studies (References 3 and 23) have demonstrated that problems can occur at the platinum-copper interface which could affect the long-term performance of the electrode. In the case of diffusion bonded or coextruded electrodes, interdiffusion between the two metals have been observed, along with the formation of Kirkendall voids. The growth of these voids can lead to localized heating and eventual separation of the platinum from the copper. Additionally, the solid solution formation of Pt-Cu due to the interdiffusion could possibly change or degrade the electrical and/or thermal properties at the interface. When a braze has been used to join the two metals, high interfacial stresses have been observed, along with evidence of volatilization and/or oxidation of some of the braze constituents. Diffusion of the braze alloy constituents into the platinum has also been detected.

These possible deleterious occurrences in the platinum-copper system are a cause for concern. Consequently, a study of the platinum/copper system was initiated, the objective of which is to examine the extent of diffusion of copper into platinum with time and temperature. Other concerns will be to observe the formation and growth of voids at the interface, measure the change of platinum concentration with time, and possibly examine any changes of thermal and electrical properties with time. An evaluation can then be made as to the extent of long term degradation of the Pt-Cu interface and potential solutions, either through improved or new fabrication techniques or refractory metal diffusion barriers, can be proposed to reduce or inhibit interdiffusion or void formation.

A literature review of current diffusion studies in the platinum/copper system was initiated. To date, there appears to be limited information on their interactions with time and temperature. The Pt-Cu phase diagram, as shown in Figure 5, shows that a continuous series of solid solutions are formed at high temperatures

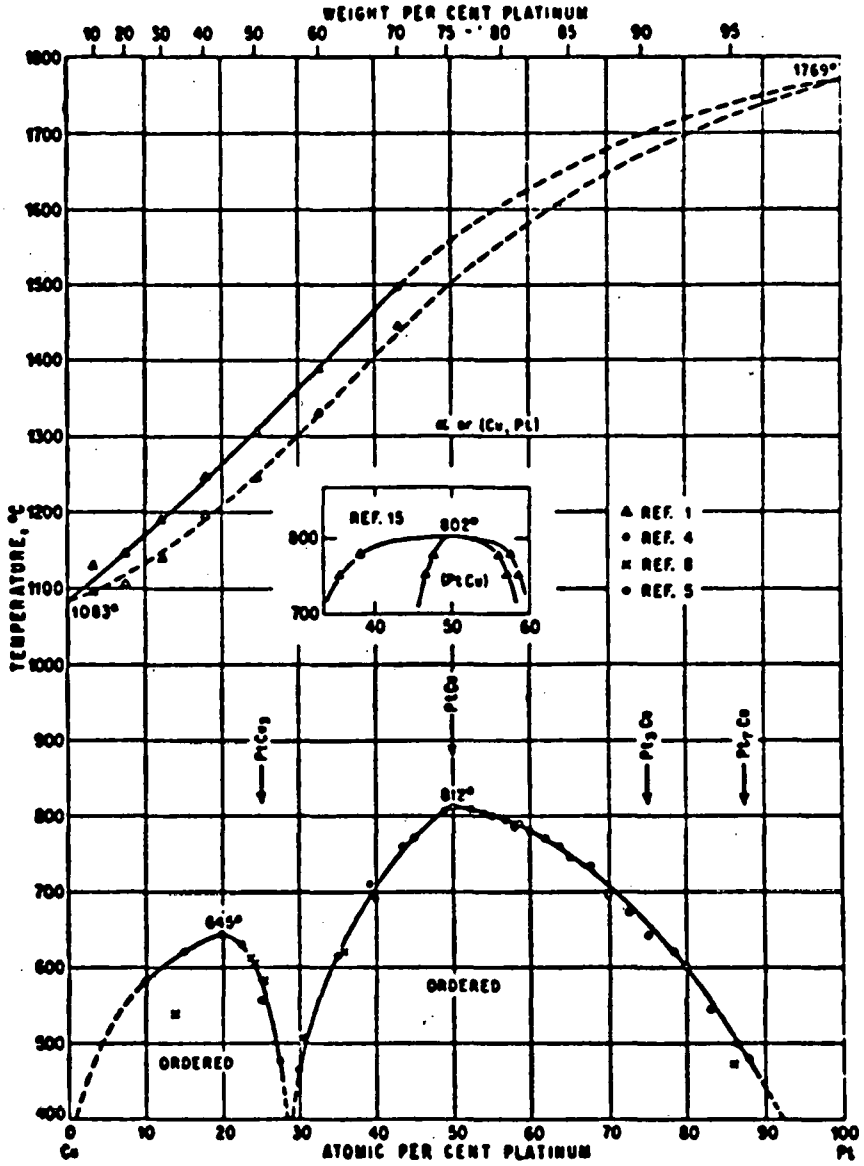

Fig. 353. Cu-Pt

Figure 5. Cu-Pt Phase Diagram (from M. Hansen, Constitution of Binary Alloys, 2nd Edition, McGraw-Hill Book Co., Inc., 1958).

Order-dis-order transformations are also detected in the lower temperature regime across a wide range of compositions. These ordered phases, if developed at a Pt-Cu interface, could influence the properties, e.g., increase the electrical resistivity and/or cause embrittlement. Scant information appears to be available on actual tracer diffusion coefficients for the Pt/Cu system. Johnson and Faulkenberry (Reference 24) are the only known investigators to have measured diffusion coefficients using tracers for both ^{64}Cu in polycrystalline platinum and ^{195}Pt in pure copper. Unfortunately, their data shows a great deal of scatter and should be treated with some skepticism. The only prior Pt-Cu interdiffusion study available is that by Ogilvie, et al (Reference 25). Their investigation noted difficulty in bonding the two metals together, as well as the development of a considerable amount of 'non-Kirkendall' porosity at the interface between the metal couple. The appearance of these voids could not be explained.

Diffusion bonding was selected as the means of quantitatively characterizing the interdiffusion between copper and platinum. The bonding was carried out in a hot-press under an argon atmosphere. Small square 0.010" thick samples 0.5" x 0.5" of both platinum and copper foil were cut and a platinum piece was sandwiched in between two copper pieces for the pressing. The copper foils were cleaned in a 5% HNO_3-95%H_2O solution and the platinum was heated in air to 1000°C for one hour just prior to their bonding. The Cu-Pt-Cu stack was fastened together with a small piece of adhesive tape on the outside surfaces to eliminate misalignment of the foils during setup. The stack was positioned in a graphite die between two graphite spacers and heated by conduction from induction heating of the graphite die by the use of a radio frequency generator. The temperature of the meal foils was monitored by using a chromel-alumel thermocouple positioned in close proximity to the Pt-Cu interface.

The intial bonding objective was to reach a baseline Pt/Cu attachment with minimal interdiffusion. Annealing experiments could then be run to assess the extent of interdiffusion as a function of time and temperature. A series of bonding trials were made at various hot-press test conditions, as listed in Table 4. The samples were slowly cooled from their test temperatures and metallographically mounted perpendicular to the pressing direction. Each specimen could then be ground and polished to expose the Pt/Cu interface.

TABLE 4

PLATINUM/COPPER INTERDIFFUSION AT DIFFERENT HOT PRESSING CONDITIONS

TRIAL NO.	TEMPERATURE (°C)	TIME ⊛ (MIN)	PRESSURE (PSI)	ΔX INTERDIFFUSION* ZONE (μm)	COMMENTS
1	500	1	2500	---	Poor bond, wide separation between Pt and Cu.
2	500	45	2500	3.5	Some separation in spots.
3	500	300	1000	15	Separation is observed in a few areas.
4	600	1	2500	4.5	Good bond
5	600	10	2500	6.0	Good bond
6	850	15	1000	9.5	Good bond
7	850	300	1000	30	Good bond

*As measured by electron microprobe trace.

⊛ The time does not include the ~10 minutes required to reach maximum temperature.

Photomicrographs of the diffusion zones, three of which are shown in Figure 6, were taken to document any separation or void formation at the Pt/Cu juncture. Electron microprobe traces were also taken across the interface to measure the interdiffusion.

The hot pressing trials revealed that a 600°C minimum bonding temperature was necessary to eliminate gaps and separation between the platinum and copper foils. Figure 7 illustrates the incomplete diffusion that results at a lower temperature. Higher pressures than were tried in these tests to possibly eliminate some of the separation observed below 600°C. From the hot pressing trials one set of test parameters was chosen for the annealing experiments, i.e. 600°C for 1 minute at 2500 psi. The bond achieved at these test conditions (shown in Figure 6) exhibits a diffusion zone of only 4.5 μm. The bond appears uniform along its whole length with no detectable voids. This particular bond resulted in the least amount of interdiffusion without observable separation.

A set of twelve Cu/Pt/Cu stacks were subsequently all hot-pressed at the same selected hot-press test conditions. One of the pressed 'sandwiches' was randomly selected for mounting and polishing to verify a uniform bond had been achieved. The samples are currently being annealed in a vacuum furnace for various age times and temperatures.

The interpretation of the interdiffusion between platinum and copper will consist of both metallographic examination of the interface for detection of voids, phase changes, etc., and microprobe analysis of the interface which supplies an interdiffusion concentration profile. The microprobe analysis generates a concentration versus penetration curve similar to the one shown in Figure 8. Besides the actual measurement of the Pt-Cu interdiffusion zone a Boltzmann-Matano analysis can be applied to the cure to obtain a valve for D (interdiffusion coefficient) over a range of copper-platinum compositions. The calculation of the interdiffusion coefficient, which assumes that diffusion and bulk motion are all one and the same process, is important in that it expresses a relationship between composition, penetration and time. D can be obtained from the graphical integration and differentiation of C(x) using the equation

$$D = \frac{-1}{2t} \left(\frac{dx}{dc}\right)_{C_1} \int_0^{C_1} x \; dc \qquad (1)$$

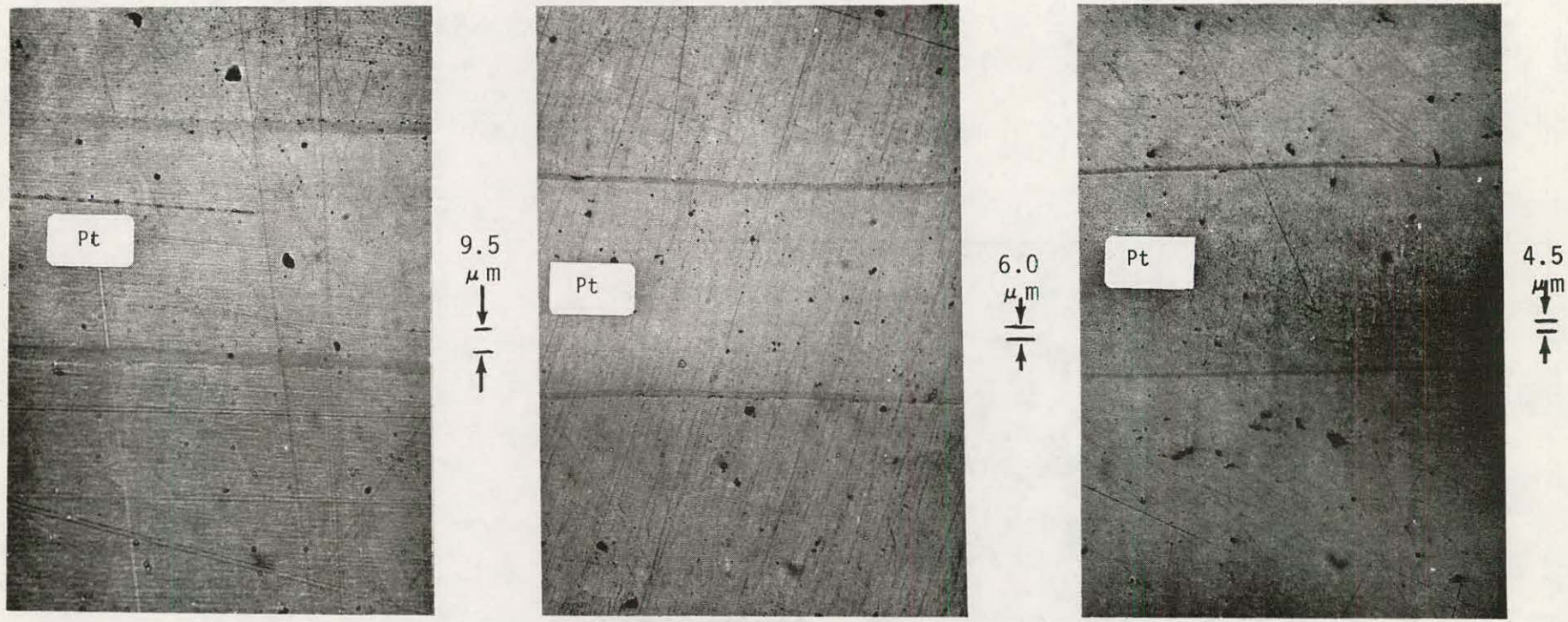

850°C
1000 psi
15 Min.

600°C
2500 psi
10 Min.

600°C
2500 psi
1 Min.

Figure 6. Diffusion of Copper into Platinum at Different Test Conditions (176X)

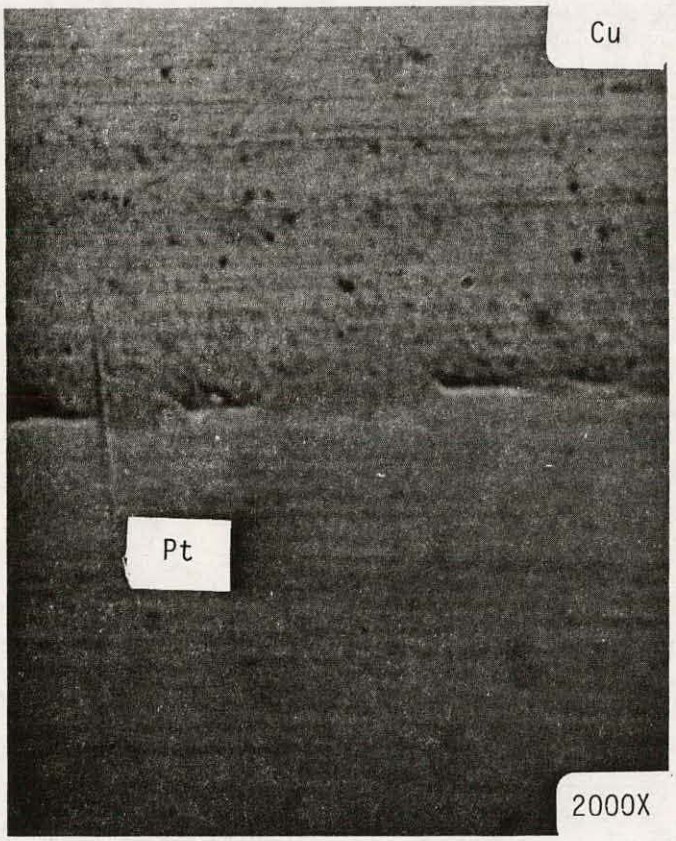

Figure 7. Copper/Platinum Diffusion Bond Hot Pressed at 500°C for 5 Hours at 1000 psi in Argon. (Note the Voids at the Interface)

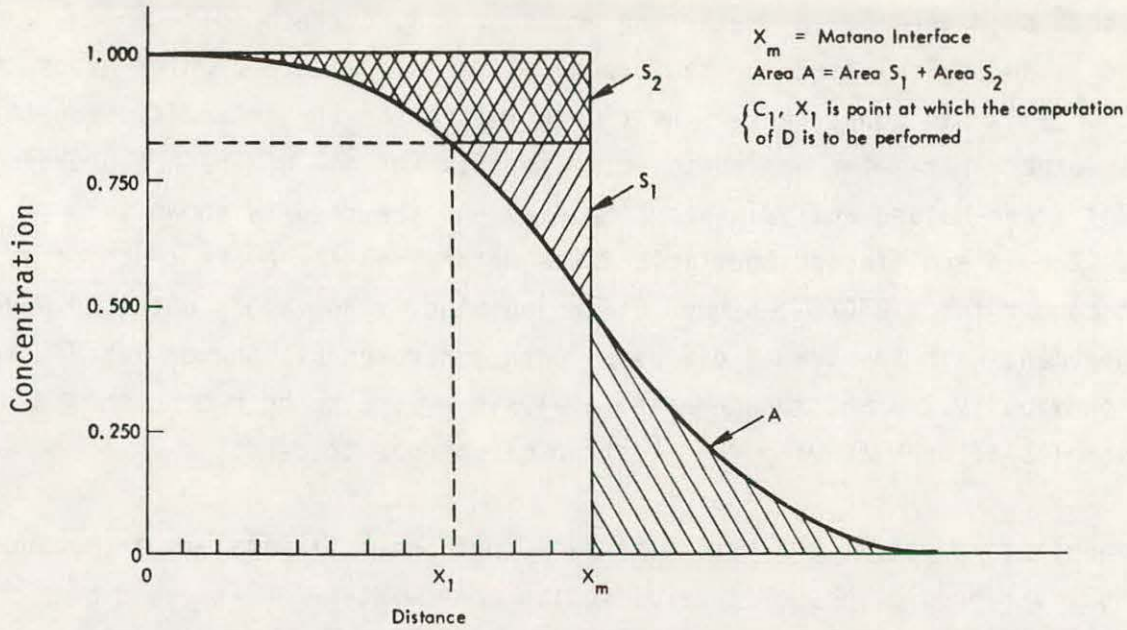

Figure 8. Schematic Concentration-Penetration Curve for a Semi-Infinite Diffusion Couple, Boltzmann-Matano Analysis

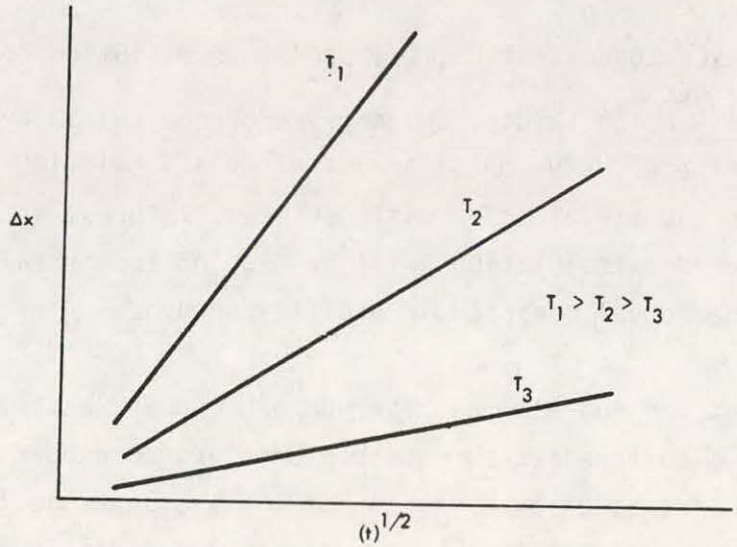

Figure 9. Predictive Extrapolation of Interdiffusion Zone Width (ΔX) as a Function of Age Time (t) for Varying Temperature (T)

As shown in Figure 9, the solution for D is based on first determining the Matano interface, the plane at which x = 0. Graphically, this is the line that makes Area A = Area S_1 + Area S_2. D for a particular concentration, such as C_1, could then be determined by measuring Areas S_1 + A, corresponding to $\int_0^{C_1} x\, dc$, in Equation 1, and calculating the reciprocal of the slope at C_1, which gives the solution to $\left(\frac{dx}{dc}\right)_{C_1}$ in Equation 1. The time allotted for the interdiffusion (t) is the only other parameter needed to solve for D. For one of the hot-pressing trials a Boltzmann-Matano analysis was completed and the results shown in Figure 10. The interdiffusion coefficient was determined for every tenth of a wt percent copper for a 850°C , 5 hour diffusion bond. The values obtained were in good agreement with the tracer diffusion data generated by Johnson and Faulkenberry mentioned previously. A Boltzmann-Matano analysis will also be run on the annealed samples after receiving the electron microprobe tracers.

Another important aspect of the interdiffusion coefficient is its use in making engineering level predictions of interdiffusion zone widths for extended age times. If a D is known for a specific diffusion temperature and composition, then the interdiffusion depth can be predicted by the following expression:

$$\frac{C_o - C}{C_o} = \text{erf} \frac{x}{2\sqrt{Dt}} \qquad (2)$$

where $\frac{C_o - C}{C_o}$ is the Pt-Cu concentration, D is the interdiffusion coefficient t is the age time, x is the zone width, and erf (Reference 26) an error-function solution. This can ultimately give one a series of curves relating total penetration distance versus age time for different temperatures, as depicted in Figure 9. These predicted extrapolations will be made on the annealed samples as a comparison with the actual measured interdiffusion zone.

Besides studying the interaction between platinum and copper, a series of refractory metals were also screened as possible barriers to copper diffusion. The work was initially undertaken by S. K. Lau of the Westinghouse R&D Center who hot-pressed six refractory metals in between copper and platinum foils. The testing conditions were 800°C, 1 Ksi for five hours. Photomicrographs of three of the metals, namely, hafnium, zirconium, and titanium, revealed extensive cracking and separation at both the platinum and copper interfaces. The other

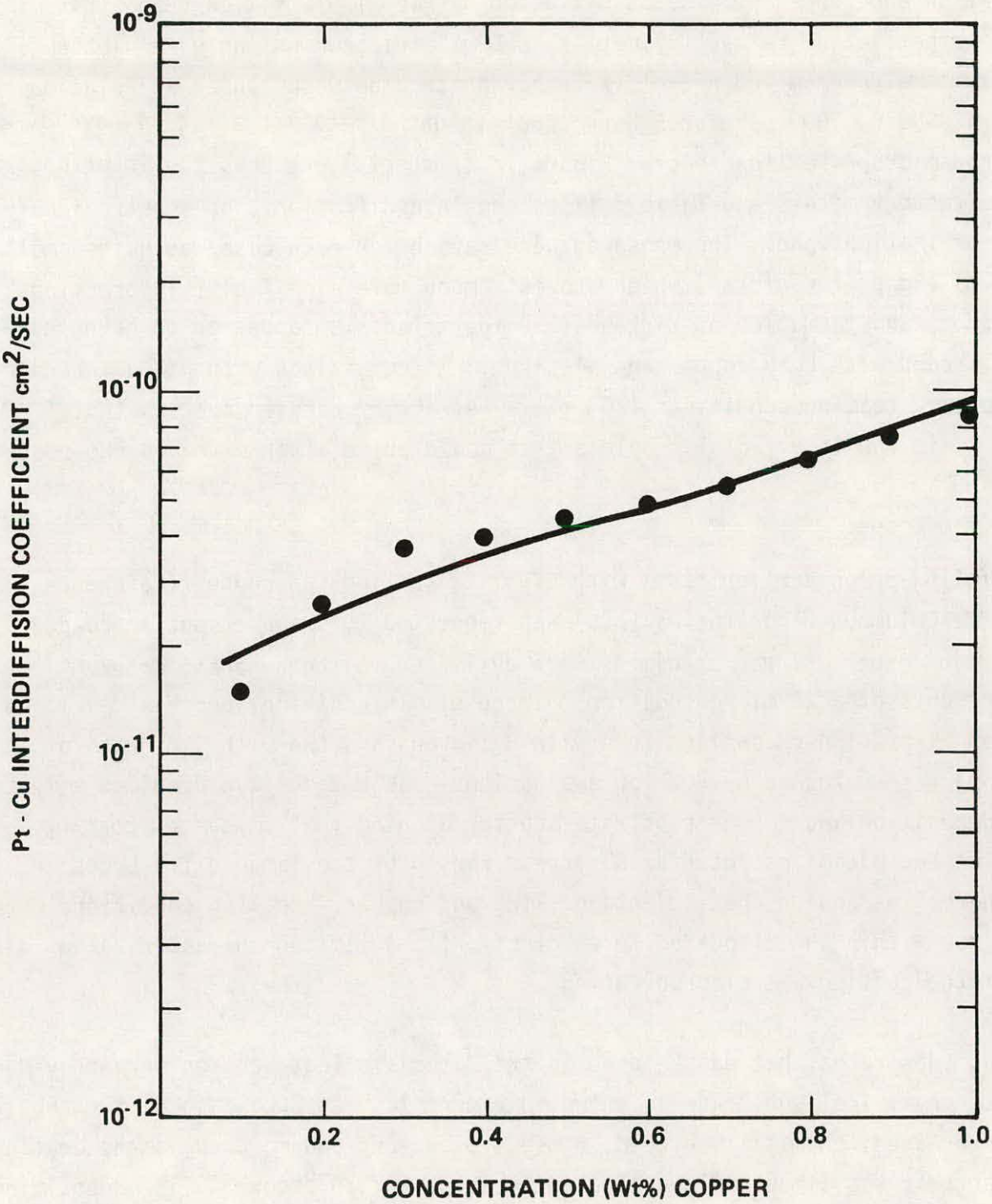

Figure 10. Platinum-Copper Interdiffusion Coefficients for Diffusion Bond at 850°C for 5 Hours

three, niobium, tantalum, and molybdenum, exhibited little visual evidence of separation and showed promise as diffusion barriers. To follow up on this work another set of refractory metals, 2-5 mil thick which included niobium, tantalum, molybdenum and nickel, were hot-pressed between copper and platinum foils at 850°C, 1000 psi for 5 hours and evaluated metallographically and by an electron microprobe line trace. Figure 11 (2 sheets) presents the interfaces of the refractory metals and Table 5 lists the interdiffusion zone penetration for each combination bond. The measured penetration for each case was quite small (1-3 μm) except for nickel, which showed a much more significant interaction (12-15 μm) and formation of Kirkendall voids. Tantalum appeared to have the best overall bond with both copper and platinum. In comparison with Pt-Cu interdiffusion at the same testing conditions (20 μm), a refractory barrier such as tantalum could limit the interfacial problems that could arise after extended MHD operations.

TiB_2 Clad Copper

As a follow-up on earlier tests with CVD TiB_2 coatings on copper (Reference 4), Battelle-Columbus Laboratories (BCL) was requested to prepare sputter coated TiB_2 clad copper. Three specimens were delivered to the purchase order requirements of a 20 micron coating thickness. In addition, process development samples with thinner coatings (one with 8 microns and two with 2 microns of coating) were returned by BCL for evaluation. BCL's technique provided simultaneous TiB_2 deposition and copper substrate sputter etching that maximizes coating adhesion and minimizes interfacial stress caused by the large differences in the thermal expansion coefficients of TiB_2 and copper. Coating conditions were optimized within the allocated level of effort. A limited characterization of one of the coating was also performed.

Coating substrates that can be used in the Materials Test Section were provided to BCL. A typical substrate is shown in Figure 12. At BCL, each of the substrates were degreased, chemically etched, rinsed, blown-dry and mounted in the coating chamber that was immediately evaluated to about 2×10^{-6} torr. TiB_2 deposition was carried out with an RF sputter cleaned TiB_2 target to substrate distance of 5 cm and an argon pressure of 20 microns. RF power applied to the 5 cm diameter target was 750 watts. Deposition parameters are summarized in Table 6. The bias voltage needed to achieve the desired graded layer of TiB_2-Cu was

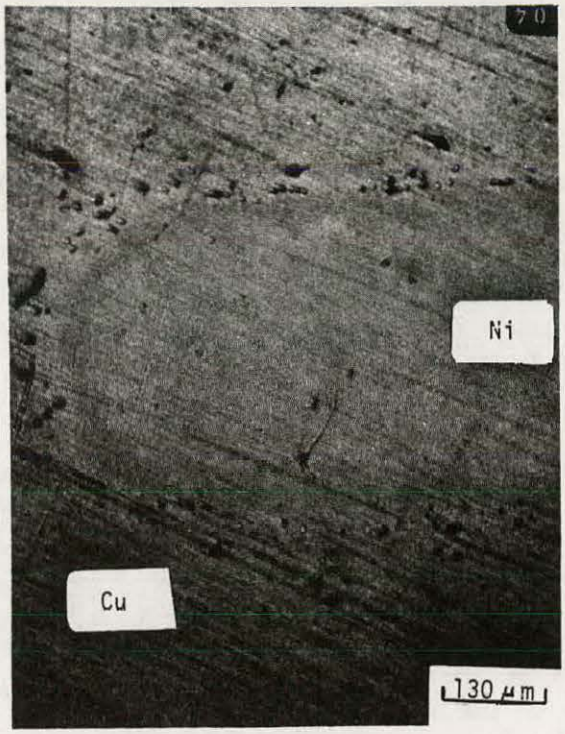

(A) NICKEL

(B) NIOBIUM

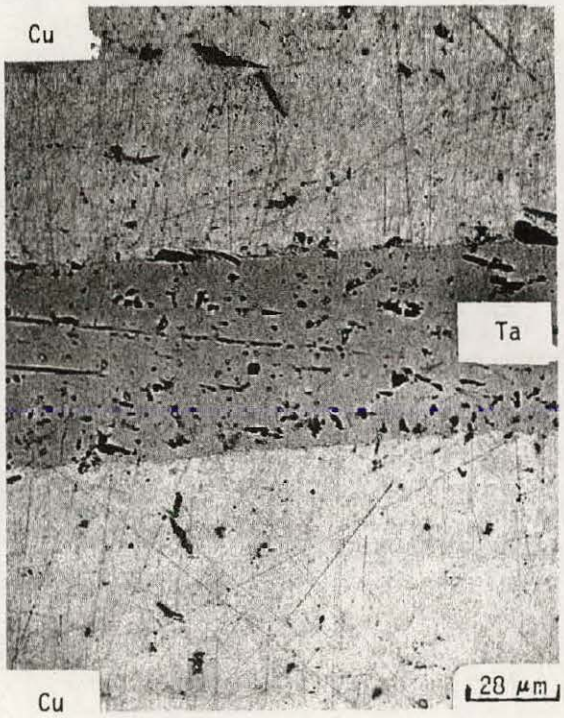

(C) TANTALUM

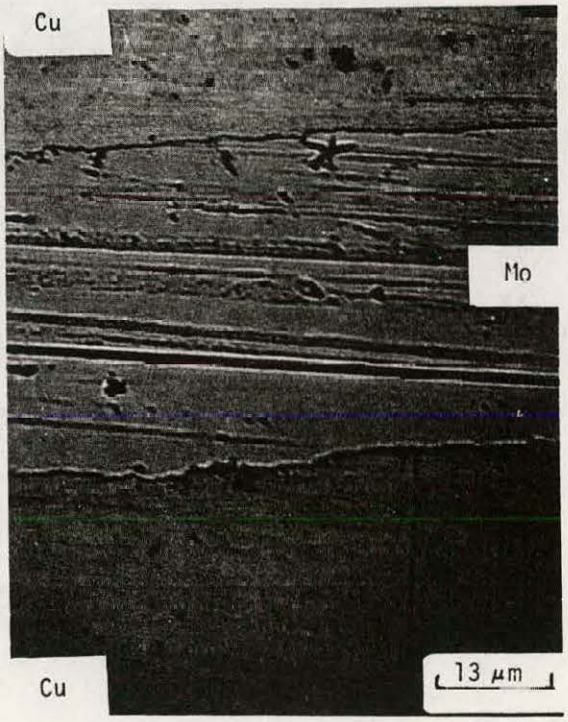

(D) MOLYBDENUM

Figure 11. Interdiffusion Zone Between Copper and Four Refractory Metals (after 850°C, 1000 psi for Five Hours)

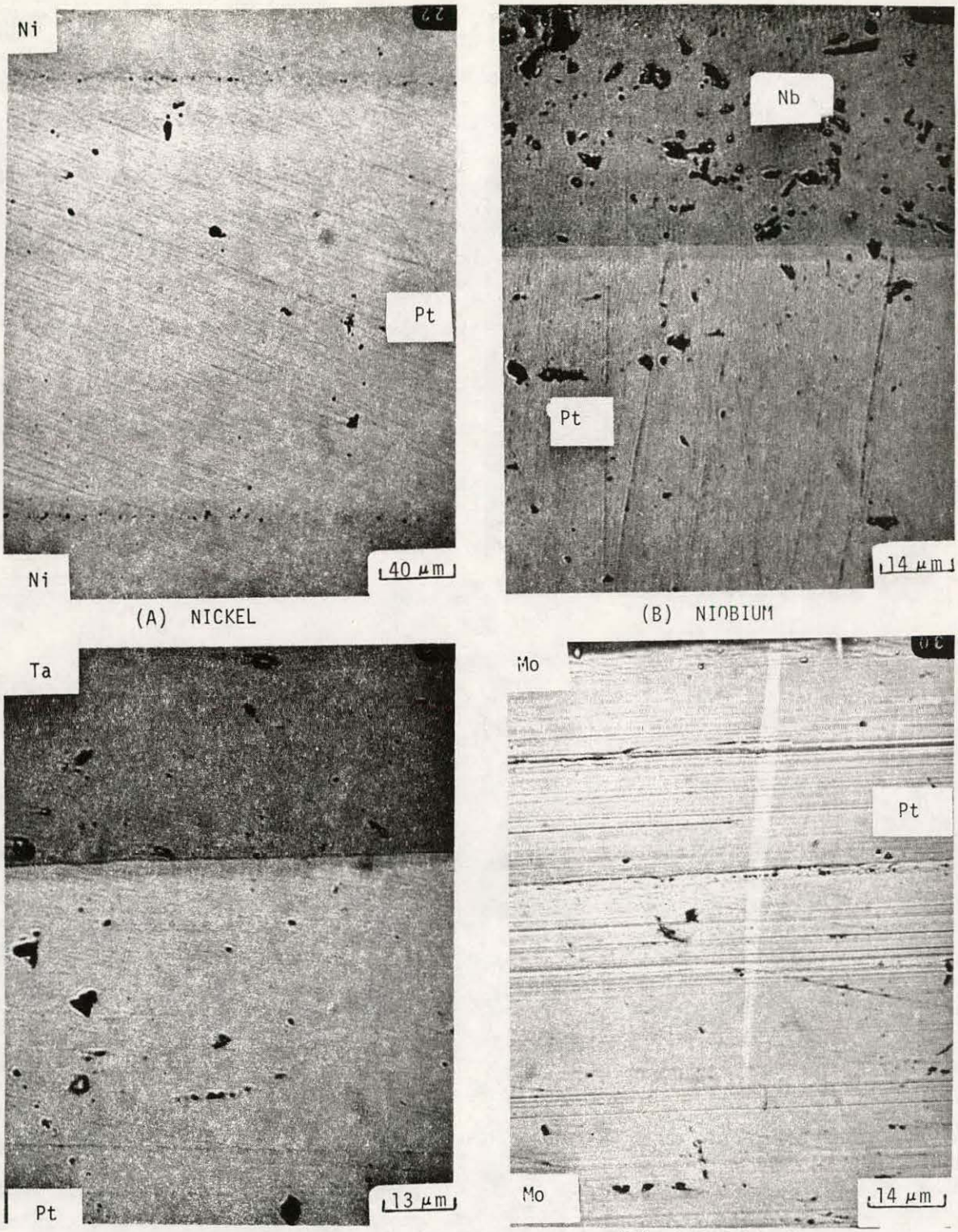

(A) NICKEL (B) NIOBIUM

(C) TANTALUM (D) MOLYBDENDUM

Figure 11. Interdiffusion Zone Between Platinum and Four Refractory Metals (after 850°C, 1000 psi for Five Hours)

TABLE 5

ELECTRON MICROPROBE INTERDIFFUSION PENETRATION ANALYSIS
AFTER 5 HOURS AT 850°C, 1000 PSI

METAL COUPLE	AVERAGE INTERDIFFUSION ZONE, ΔX (μm)	METALLOGRAPHIC COMMENTS
Copper-Nickel	15.8	- Formation of Kirkendall voids is apparent
Copper-Niobium	1.25	- Good bond, slight interaction
Copper-Molybdenum	2.25	- Some separation at the interface
Copper-Tantalum	2.00	- Good bond, slight interaction
Copper-Platinum	29.0	- Some evidence of Kirdendall voids
Platinum-Nickel	12.2	- Obvious formation of Kirkendall voids
Platinum-Niobium	1.50	- Penetration into Pt appears more than actual microprobe measurement
Platinum-Molybdenum	1.00	- Some clustering of voids at interface
Platinum-Tantalum	2.25	- Good bond, slight interactions

Figure 12. Specimen for Materials Test Section

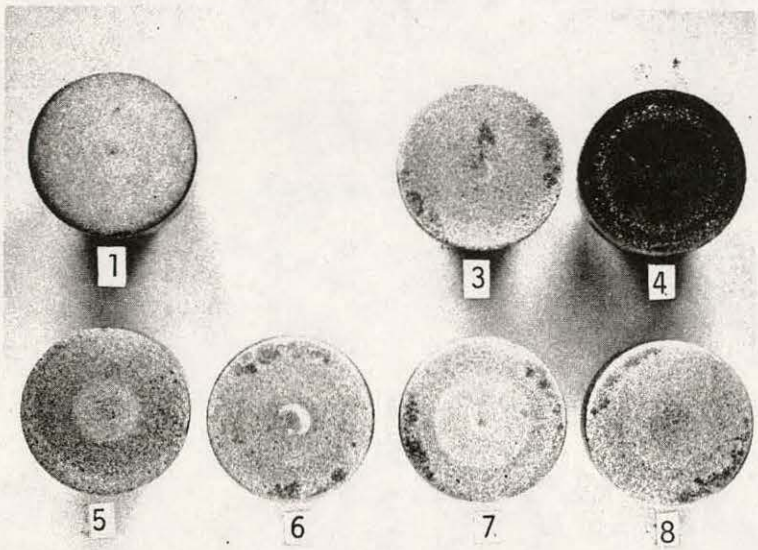

Figure 13. Surface of TiB_2 Clad Copper Specimens from BCL

TABLE 6

DEPOSITION PARAMETERS, TiB_2 ON COPPER

SAMPLE	DC BIAS ON SUBSTRATE, (kV)	DEPOSITION TIME WITH BIAS, (hr)	TOTAL DEPOSITION TIME (hr)	ESTIMATED THICKNESS, (μm)
1	0	-	2	2
2	6	0.5	2	1.8
3	3	0.5	2	2
4	Varied, Surface Sputter Etched		-	-
5	3 1	0.25 0.25	7	8
6 (Day 1) (Day 2)	3 1 1	0.25 0.25 2 min.	8.25 8	20
7	Same as 6		16.5	20
8	Same as 6		16.7	20

examined using samples 1 through 4. Above a 3 kV bias, sputter etching of the copper was occurring at a rate high enough to preclude deposition of TiB_2. In view of these observations, the fifth sample was bias sputtered with a 3000 volt bias for 15 minutes to sputter etch the surface. Some initial deposition of TiB_2 was noted. The bias voltage was decreased to 1000 volts at which point a definite coverage of the copper substrate was occurring. After 15 minutes the substrate was grounded and the deposition was allowed to continue for another 6.5 hours. The uniformity and adherence of the coating appeared satsifactory.

Samples 6, 7 and 8 were then set up to deposit a coating of TiB_2 of the desired thickness using the above procedure. Since the deposition time had to be extended over a period of two days, a short two-minute bias sputtering was carried out on the beginning of the second day in order to remove any oxide which might have formed overnight. A photograph of the coated samples is shown in Figure 13.

Further studies of the TiB_2 coating, carried out on sample 2 are discussed below:

(1) Texture: The effect of sputter etching can be seen in Figure 13 by comparing Sample 1 (zero bias) with the other samples; Sample 1 has a shiner and smoother appearance than any of the other samples. Also, this sample does not exhibit ring patterns as do several of the others. These patterns are most evident in samples 5 and 7 and are due to the nonuniform electric field distribution around the edge of the specimen which causes sputter etching rates to vary across the substrate surface. A difference in texture is observed by SEM, between the inner regions and the outer ring as shown in Figures 14 and 15. The outer region is clearly smoother but still exhibits the effects of sputter etching.

(2) Cross-section: Figure 16 shows a cross section with a magnification of 1000x. The surface roughness is clearly apparent. The coating thickness of 1.8 μm was used in estimating the values listed in Table 6.

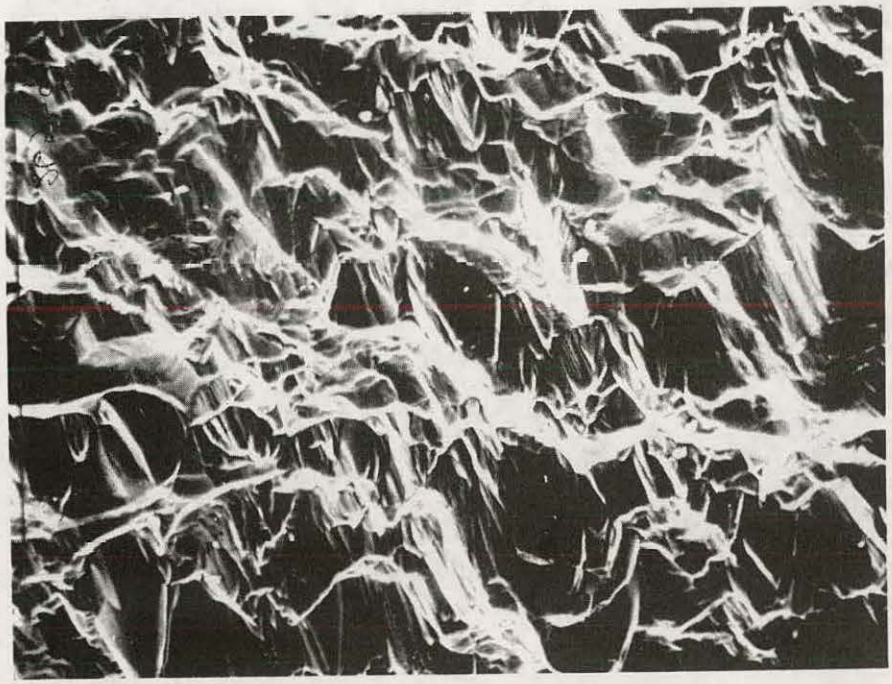

300X

Figure 14. Scanning Electron Microscope Photograph of the Central Region of Sample 2

300X

Figure 15. Scanning Electron Microscope Photograph of the Outer Ring of Sample 2

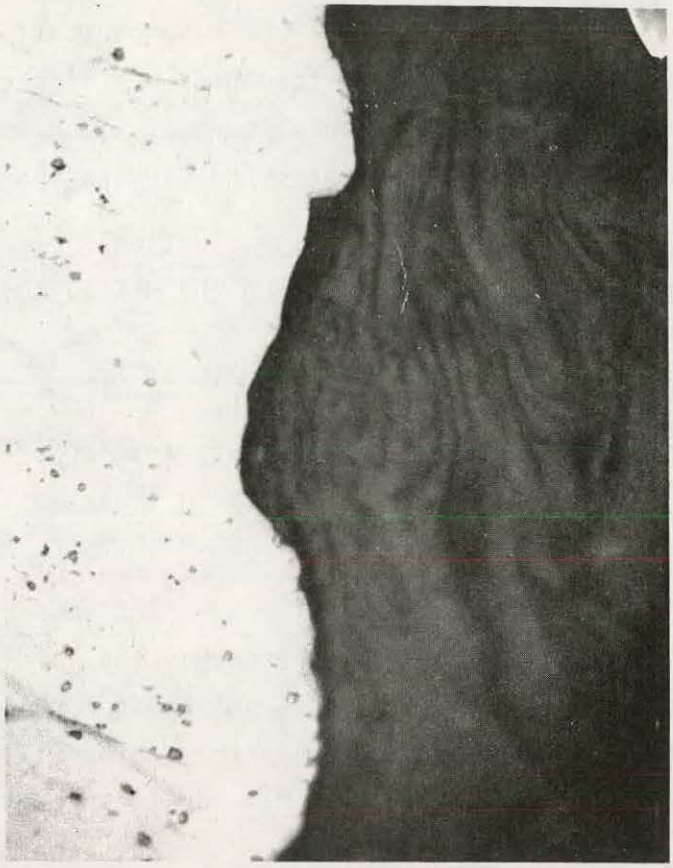

1000X

Figure 16. Photograph of a Cross Section of Sample 2

The coating is shown by the light gray path down the middle of the photograph with the lighter area showing the copper substrate

(3) X-ray diffraction: All peaks in the diffraction pattern, except one corresponding to a d-spacing of 2.32 Å, may be attributed to the copper substrate. The extra peak can be associated with either Ti or TiB, but not TiB_2. This is an indication that the sputter deposition may have depleted the boron concentration. Although the exact structure cannot be ascertained from a single diffraction peak, the coating is probably a mixture of titanium-boron phases. The appearance of a peak indicates the TiB_x coating is polycrystalline.

These specimens will undergo a more detailed evaluation including the anode arc erosion test and future testing in WESTF using the MTS II test section.

Insulator Materials

No significant laboratory scale slag compatibility testing of insulator materials was completed during the reporting period.

Attachment Techniques

A systematic study of bonding techniques is underway and is directed towards improving the reliability of ceramic to metal joints in MHD electrodes. This work is supportive of several hot electrode systems which will be supplied by Battelle Pacific Northwest Laboratories and MIT for inclusion in future WESTF tests.

A literature review of ceramic to metal attachment techniques applicable to MHD systems was completed. Conclusions drawn from the search suggest that if a conventional brazing operation is used in bonding ceramics to metals, the ceramics should first be metallized with a refractory metal prior to the application of a secondary metallic wetting layer to achieve a strong tight bond. Prior electrode attachments had relied on either a direct bond between the ceramic electrode and metal substrate using a reactive braze alloy or the metallization of the ceramic electrode with only a single (copper or nickel) metal layer prior to brazing. Consequently, work was begun on metallizing ceramic electrode materials supplied by BPNL and MIT with different refractory metals. The metallization will be applied by sputtering, plasma spraying or coating with a paste. Copper will then be applied over top to act as the wetting layer for the braze filler.

Initial metallographic examination of the ceramic-metal interfaces using several refractory metals indicates that using this double metallization technique is promising. Figure 17 exhibits the attachment interface between the ceramic composition $0.5SrZrO_3 \cdot 0.5(Sr_{.25}La_{.75}FeO_3)$ supplied by MIT and a 40% dense copper metal mesh. Here only a single copper metallization was applied. The bond looks very good in certain areas but gaps and voids are also apparent which would certainly weaken the overall attachment. This has been a common occurrence when a single metallization has been used in attaching a dense ceramic to a metal. On the other hand, Figure 18 exhibits the attachment of 30 m/o In_2O_3-20% m/o $PrO_{1.8}$-3.0 m/o Yb_2O_3-47m/o HfO_2 supplied by BPNL. In this case a platinum coating was first applied to the ceramic prior to sputtering a layer of copper. The bond appears to be very continuous with adhesion evident whenever there is contact between the ceramic and copper mesh. The double metallization would appear to offer greater wettability at the interface, which is definitely desirable when dealing with a metal mesh that results in reduced surface area for attachment. Continued evaluation of these bonding techniques will include tensile testing of typical specimens to gain some information on the relative strength of the different attachments.

1.1.2 Material Characterization

Thermal Conductivity

The thermal conductivity of the type MMM ceramic current leadout was determined by BPNL. The material was processed by BPNL and is to be run in a future super-hot WESTF test. The thermal diffusivity was measured using a laser pulse technique from near room temperature to temperatures up to 1400°C. The thermal conductivity, as shown in Figure 19, was calculated from the thermal diffusivity, room temperature density, thermal expansion and the specific heat.

The data taken on heating was used to plot the curve. The conductivity is relatively temperature independent below 1000°C, which is the anticipated design temperature range. The average value between 291 and 1020°C is $2.63 \begin{smallmatrix}+0.14\\-0.06\end{smallmatrix}$ watts/MK. The variation represents an error of $\pm$ 5% which is also the quoted absolute error for the measurements.

Figure 17. Attachment of 0.5 $SrZrO_3 \cdot 0.5\ (Sr_{.25}La_{.75}FeO_3)$ to Copper Mesh (Surface of Ceramic was Sputtered with 7 Microns Copper and Brazed with BT for 2.5 minutes at 10^{-5} torr)

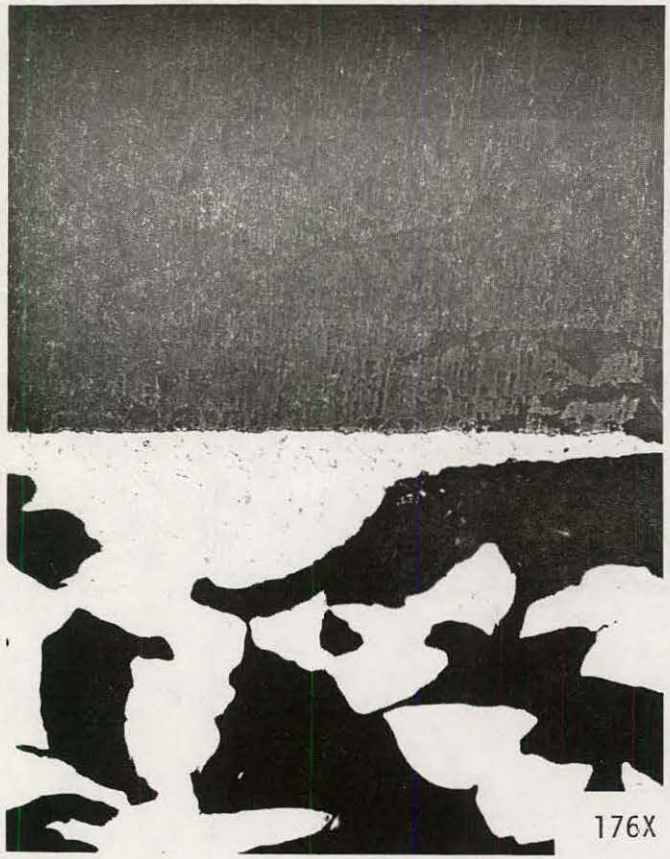

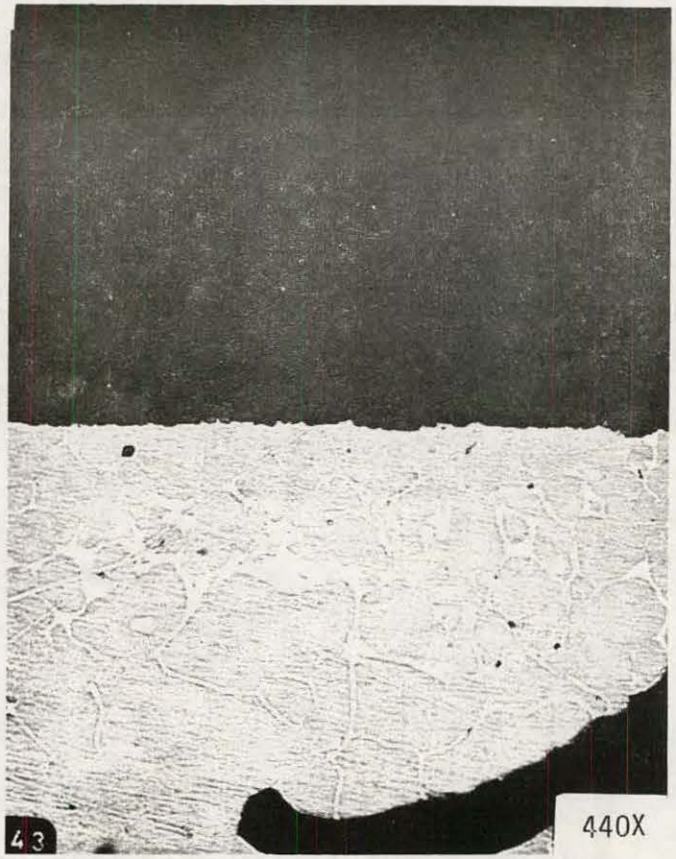

Figure 18. Attachment of 30 m/o In_2O_3-20 m/o $PrO_{1.8}$-3.0 m/o Yb_2O_3-47 m/o HfO_2 to Copper Mesh (Surface of Ceramic was Coated with Pt Paste and then Sputtered (6μm) with Copper Prior to Brazing with BT)

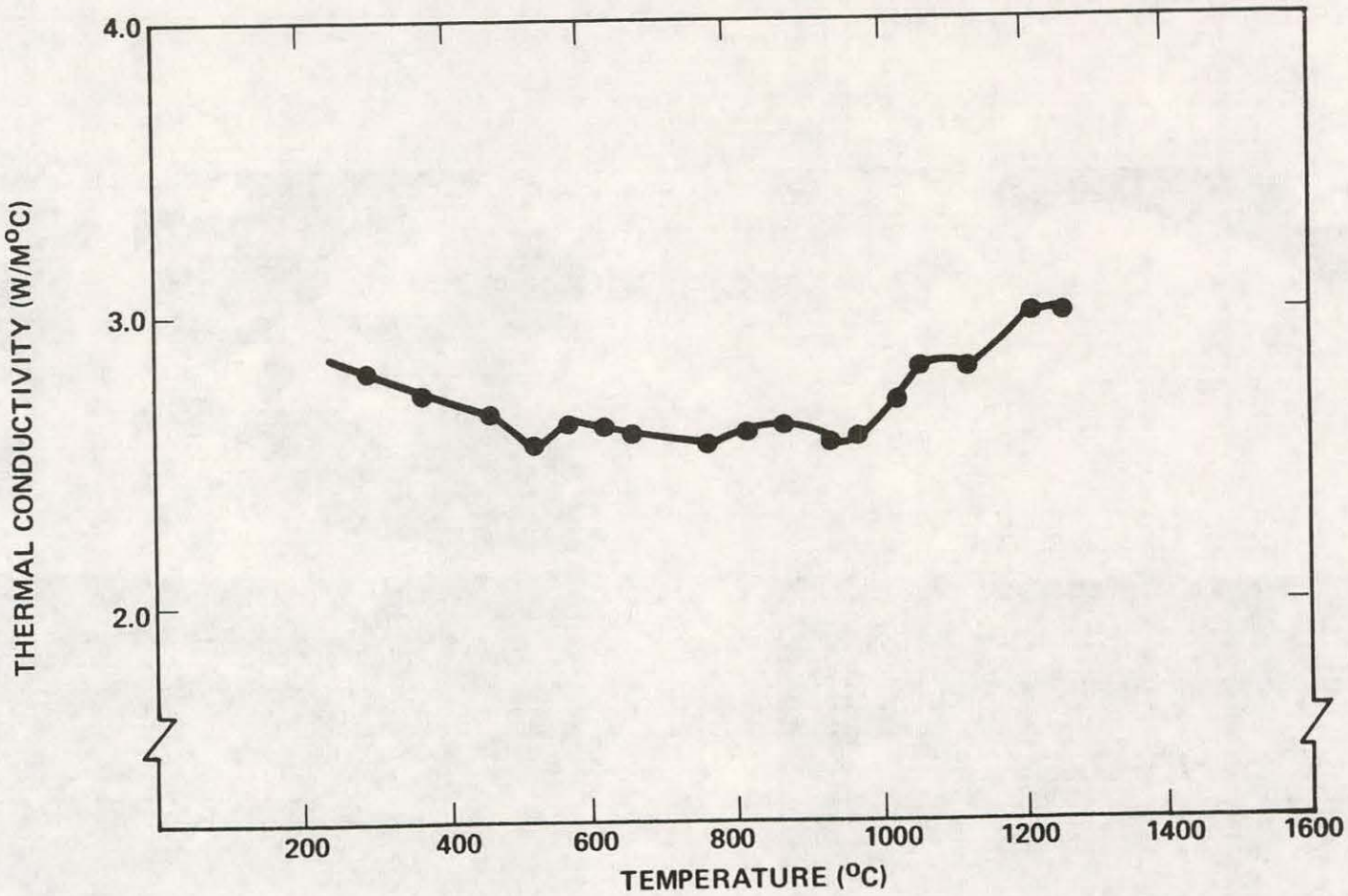

Figure 19. Thermal Conductivity Type MMM Ceramic

1.2 WBS 1.1.2 - Laboratory Screening Tests

1.2.1 Electrochemical Corrosion Tests

No significant electrochemical corrosion testing was completed during this reporting period.

1.2.2 Anode Arc Erosion Studies

Laboratory investigations are continuing towards developing a consistent anode arc erosion test to be used for screening cold wall anode materials. The latest version of the arc erosion test, shown schematically in Figure 20 differs from the prior arrangement in that an oxy-acetylene torch and an arc deflector have been added. The oxy-acetylene torch is used to heat the surface of the test sample. The torch not only permits the sample to be heated to temperatures greater than that attainable with the arc alone, but it partially melts the corrodents which are dusted on the sample thereby allowing them to adhere longer to the surface. The magnetic arc control (MAC) is used to deflect the arc and cause it to sweep over the sample surface at a controlled velocity. It is believed that such arc motion provides a better simulation of the conditions in a real MHD channel.

In the test, the 2.5 cm diameter test button is rotated at 1 rpm and is heated by the flame from the torch while a magnetically deflected arc ($\pm$ 1/2 cm deflection at 46 cycles/minute) plays over the sample surface. The arc is generated by a plasma needle arc welding unit and is maintained at a constant 5.5 amps over the 2 hour test duration. Voltage drops are approximately 20-28 volts. The test is isothermal and temperatures in the range 250°-600°C, maintained by cooling the back face of the arc button, have been investigated. The corrodent is dusted onto the sample surface in solid powder from (-200 mesh) every 15 minutes in 1.5 gm increments.

Test buttons are made of either pure OFHC copper or copper on which 0.25-0.75 mm foils of potential anode metals (i.e., Pt, superalloys, etc.) are silver brazed. After testing, the sample buttons are cleaned in a 10:1 solution of H_2O:HF, dried and weighed to obtain corrosion weight loss data. Corrections are made for weight losses occurring on the sides of test samples, and all data is reported as weight changes on the arc button surface directly impinged by the arc.

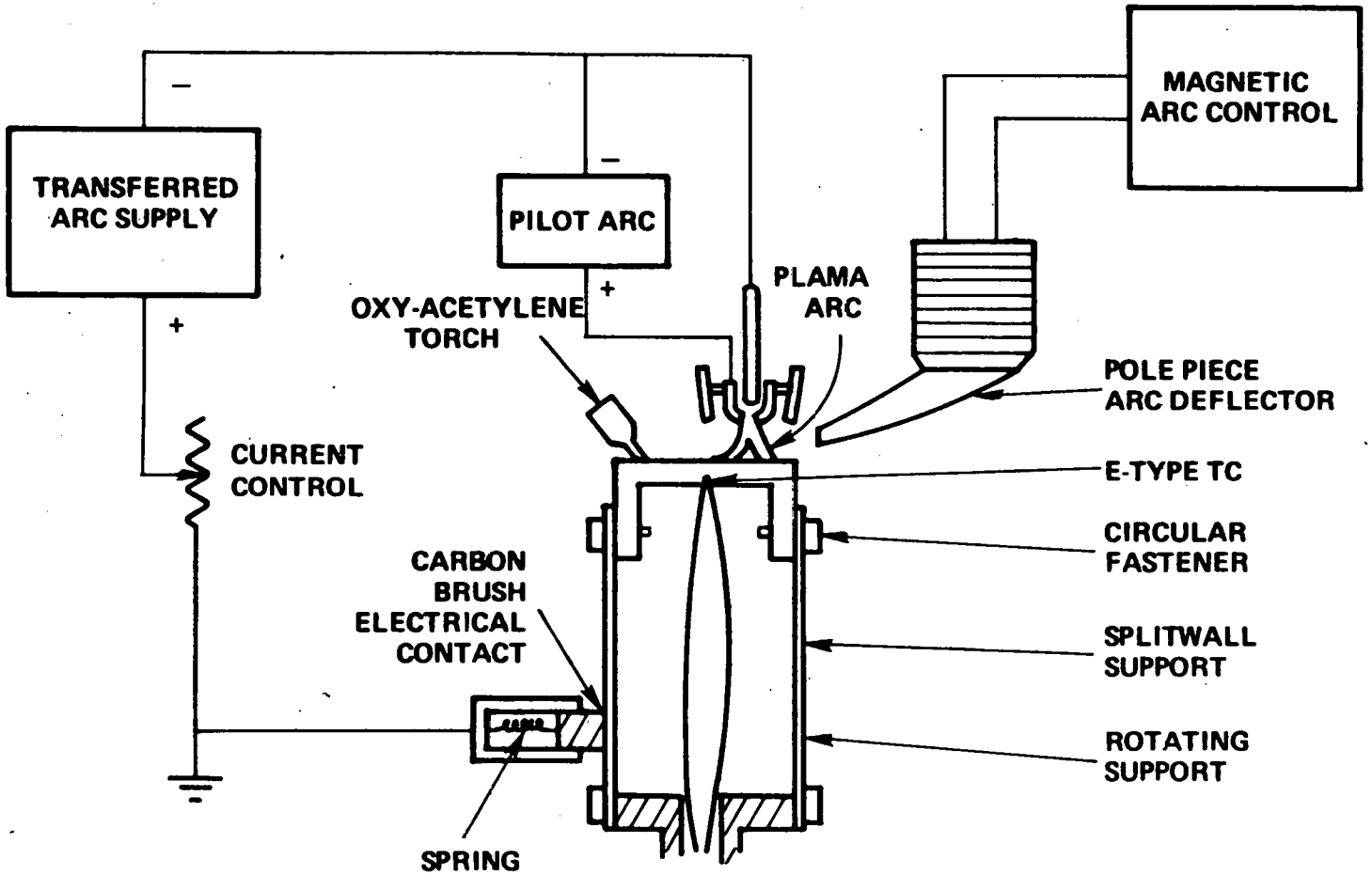

Figure 20. Schematic of New Anode-Arc Corrosion Test

It was found relatively early in these laboratory tests that corrosion of bare copper was very sensitive to the rate at which the corrodent was dusted on the sample surface and on how rapidly the non-adherent corrosion reaction products were removed*.

For example, applying 1 gram of K_2SO_4 every 15 minutes and removing the products every 20 minutes in a 500°C, 2 hour arc test gave copper weight losses of about 3 grams. Doubling the amount of K_2SO_4 applied increased corrosion losses about 2.5 times. Halving the time between removing the reaction products generally increased corrosion losses about 1.5 fold. The present standardized procedure is to apply 1.5 grams K_2SO_4 every 15 minutes and to remove the reaction debris every 30 minutes. It is not yet known if this procedure is an optimum one. However, it does permit us to obtain self consistent weight loss results that are reproducible with copper to $\pm$ 5%.

Using the standardized procedures, a series of experiments have been run with copper samples to evaluate the role of thermal, chemical and arc effects on corrosion. These tests involved: a) heating samples only with a torch (thermal-oxidation effect); (b) heating samples with torch in presence of corrodents (thermal-chemical effects); (c) heating samples with torch and arc (thermal-arc effects); and (d) heating samples with torch and arc in presence of corrodents** (thermal-chemical-arc effects).

The results are shown in Figure 21. It is clear from this data that gross thermal effects alone (dashed curves) are not very important in corrosion. In the worst case, thermal corrosion with K_2SO_4 corrodent results in only 0.07 gm loss at 500°C. However, for the same average surface temperature the imposition of an arc increases corrosion nearly 40 fold to 2.65 gms. This arc accelerated corrosion must be due to either the thermal spike giving rise to enhanced reaction rates at the arc spot and/or electrochemical reactions between the K_2SO_4 and the copper due to current transfer through the electrolytic corrodent. It is not possible to distinguish between these two mechanisms at present although

---

*It is necessary to regularly remove the corrosion products - otherwise, the reaction scale builds up to a sufficently thickness such that it effectively dissipates the energy of the arc. At this point, no further arc damage occurs.

**Slag is premelted W-50 flyash containing 10 w/o K_2O.

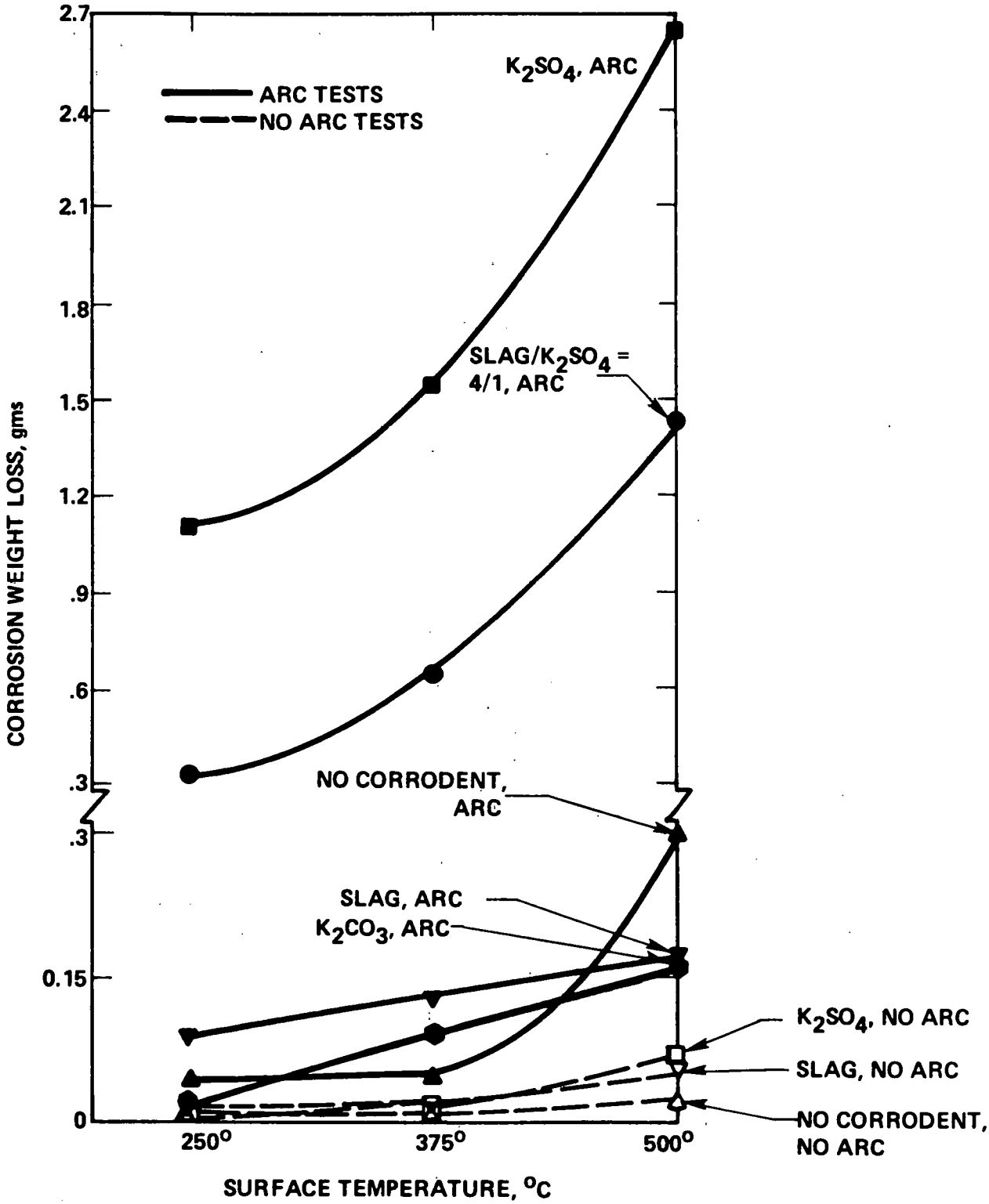

Figure 21. The Effect of Arc, Corrodents and Surface Temperature on Corrosion of Copper

it is suspected that electrochemical effects are dominant.

Other important effects shown in Figure 21 are that K_2CO_3 and sulfur free slag are relatively non-reactive with copper even in the presence of an arc and the addition of 20 w/o K_2SO_4 to slag increases arc corrosion by an order of magnitude over sulfate free slag indicating a strong dependence of corrosion on sulfate concentration. This result shows that sulfur masks out corrosion effects due to slag alone and suggests that future tests to evaluate arc corrosion resistance be run with pure K_2SO_4. It can also be noted that at 500°C, arc corrosion of corrodent free copper is more than that with slag or K_2CO_3 coated copper. Although unexpected, this result illustrates an important factor influencing arc damage i.e., the corrodent can absorb a sizeable fraction of the total arc energy. This fact was qualitatively observed in earlier arc experiments where it was found that if the surface reaction layer and/or corrodent built up to a thickness of about 1/8", no further corrosion of the underlying surface would occur.

A number of potential anode metal alloys, the compositions of which are given in Table 7, have been tested for arc corrosion resistance. The results are given in Figure 22 in terms of weight loss/coulomb. Since corrosion losses at the lower surface temperatures were normally very small, most tests were run at 500°C. Nevertheless, even at this temperature, (considering that the estimated measuring error is $\pm$ 0.008 gpm or $\pm$ 0.2 μg/coulomb) the ability to discriminate between many of the better performing materials is poor. It is obvious from Figure 22 however that copper and Inconel 600 and probably Hastelloy X can be eliminated as candidate anode materials. The experimental data indicates that at 500°C, the apparent ranking of alloys in order of increasing corrosion resistance is SS-304, E-29-4, Pt and E-26-1. However, when it is recognized that measuring errors are about $\pm$ 0.2 μg/coulomb, the certainty of the absolute ranking becomes more tenuous. Except for Pt, this list is in general agreement with AVCO data (Reference 27). It is clear that changes in present testing procedures and methods of measuring the extent of corrosion in terms other than just weight loss will be necessary to permit better differentiation between materials.

TABLE 7

COMPOSITION (W/O) OF ARC-TESTED ALLOYS

ALLOY	Ni	Cr	Fe	OTHERS
Inconel 600	77	16	7	--
Hastelloy X	46	22	19	9 Mo, 2.5 Co
SS 304	9	19	70	1.5 Mn
E-26-1	--	26	73	1 Mo
E-29-4	--	29	67	4 Mo

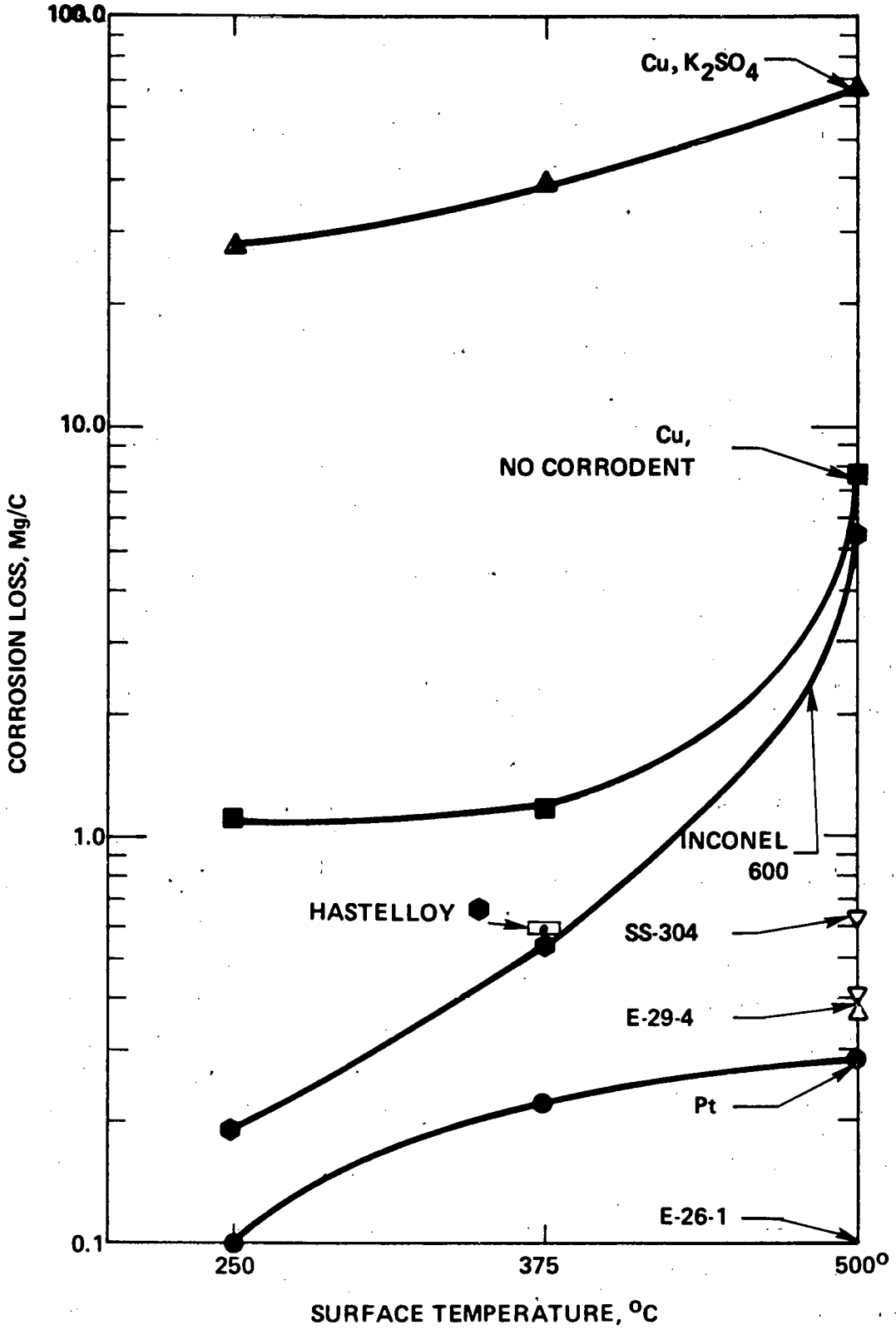

Figure 22. Anode-Arc Corrosion of Various Metal Materials

In conclusion, a modified laboratory scale anode arc corrosion test is being developed to screen potential MHD anode materials. It is encouraging that initial results are in qualitative agreement with data from AVCO in-channel tests. However, the fact that the arc test provides relatively poor discrimination between potential materials requires that certain modifications be made. Some problem areas in the test methodology which will require further development are outlined below:

1) The physical action of flame and arc tend to sweep much of the dry corrodent powder off the sample surface. A method of minimizing this effect or insuring that the amount of material remaining on the surface is the same for all sample materials is necessary.

2) At present, dry corrodent powders are hand dusted on the sample from a brush or spatula. A method of insuring that this powder does not fall in clumps, that it distributes unformly and that the same total weight of corrodent accumulates on the sample surface in all cases is required.

3) The relatively low rates of corrosion of many alloys in these tests (in some cases near experimental error) may require that longer duration and/or higher temperature tests or improved loss measurement technique be used to better distinguish between alternate materials.

4) Weight changes alone are not a sufficient measure of arc corrosion. Microscopic examination of tested samples to determine depth of corrosion attack, gain boundary reactions and the nature of the corrosion products will be necessary for a definitive ranking of anode materials.

A series of thermal analyses of the anode arc test arrangement were completed to determine the macro temperature distribution on the surface of the sample and in particular to determine the relationship between the surface temperature and the temperature at the thermocouple location. The anode arc test specimen is a one inch diameter button; the single thermocouple is located 0.010 inch from the sample surface on the sample centerline.

Heat is transferred to the sample from the plasma jet and torch via conduction and is conducted through the material and dissipated to the ambient via convection and radiation. The steady state temperature distribution for a 304 SST clad copper specimen is shown in Figure 23. Additional analyses were run for a bare copper stainless steel and an Inconel 601 clad copper specimen. In summary, the following temperature differences were predicted:

- Copper specimen ~ 2°C
- Inconel 601 clad copper ~ 6°C
- SST specimen ~ 29°C
- SST clad copper ~ 6°C

These analyses confirm that the thermocouple measurements is an accurate indication of specimen general temperature level.

2.0 WBS 1.2 - ENGINEERING TESTS

2.1 WBS 1.2.1 - Test Engineering

2.1.1 Development Requirements

During this quarter, a test matrix was being developed to reflect programmatic changes that emphasize the development and testing of cold wall electrode materials over a range of sulfur levels. Test specifications will be prepared when appropriate in response to the revised test matrix. The test matrix will provide for the demonstration of a correlation between WESTF and generator test results and for the structured evaluation of materials which are alternatives to platinum.

WESTF Tests 44, 46, and 48 for which test specifications were issued, have been deleted, and WESTF Test 50 has been redefined to be the first WESTF channel test (copper anodes) run in the rebuilt facility. This test will also provide a data point necessary to establish a correlation between WESTF and generator test results.

The design criteria for various test sections and other facility components has been documented and input is being provided to support a safety review of the facility operations.

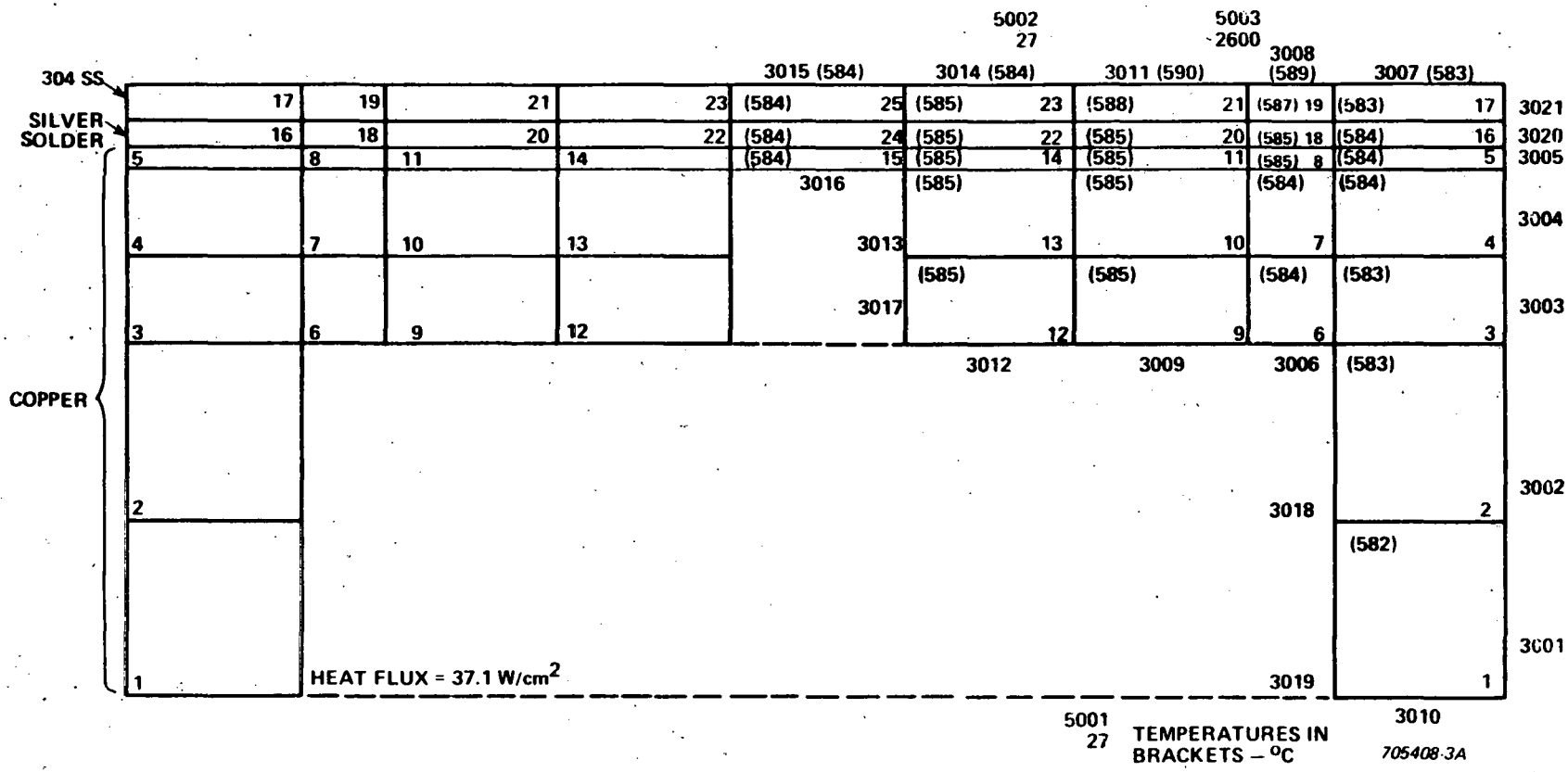

Figure 23. Steady State Temperature Distribution (°C) Copper Sample with 304 Stainless Steel Clad

2.1.2 Experiment Design

The design of the WESTF II test section was revised to emphasize the development and evaluation of slagging cold metallic electrodes. The primary constraint on the design of the test section is the available space within the magnet bore. The flow passage dimensions were established at 1.25 x 1.80 inch which includes an assumed slag layer thickness of approximately 2 mm (0.080 in.).

To improve electrical performance of the insulating sidewalls and provide better access for a viewpoint, (to observe slag formation and movement, as well as arcing phenomena) the 1.80 inch dimension was selected for the electrode separation. This will provide improved electrical performance of the sidewall and maximize viewing depth into the test section.

The following sections discuss the redesign of the MTS II and WESTF II test sections.

MTS II Test Sections

The MTS II test section that was used successfully in WESTF Tests 47 and 49 (Reference 3) will be used for the limited number of cold wall coupon tests planned in the revised test matrix. By using metal liners to adjust the channel opening to the proper cross-section, this test section can be readily adapted for screening cold wall electrode materials with the new channel geometry. The MTS unit has been cleaned and refurbished and is available for this modification.

The hot wall MTS II test section was described in Reference 3. The detail design of the basic unit has been completed, but further design efforts and fabrication activities have been deferred.

WESTF II Test Section

The basic design of the WESTF II test section has been completed. Layouts of the transverse and longitudinal views of the test section, as planned for the initial sequence of cold wall tests, are shown in Figures 24 and 25. For the initial test, WESTF Test 50, there will be eight electrode pairs in the

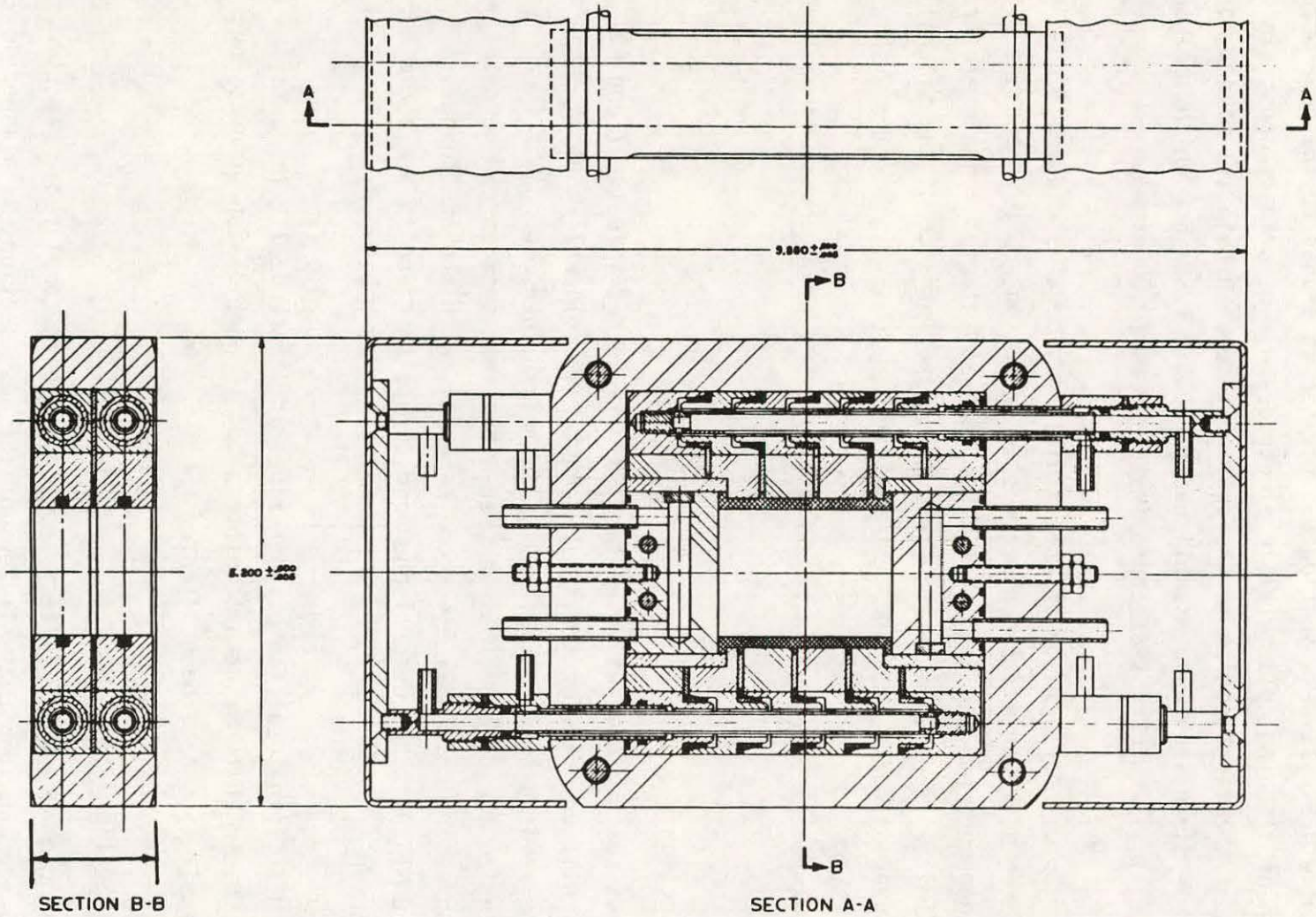

Figure 24. Typical WESTF Test Section Frame

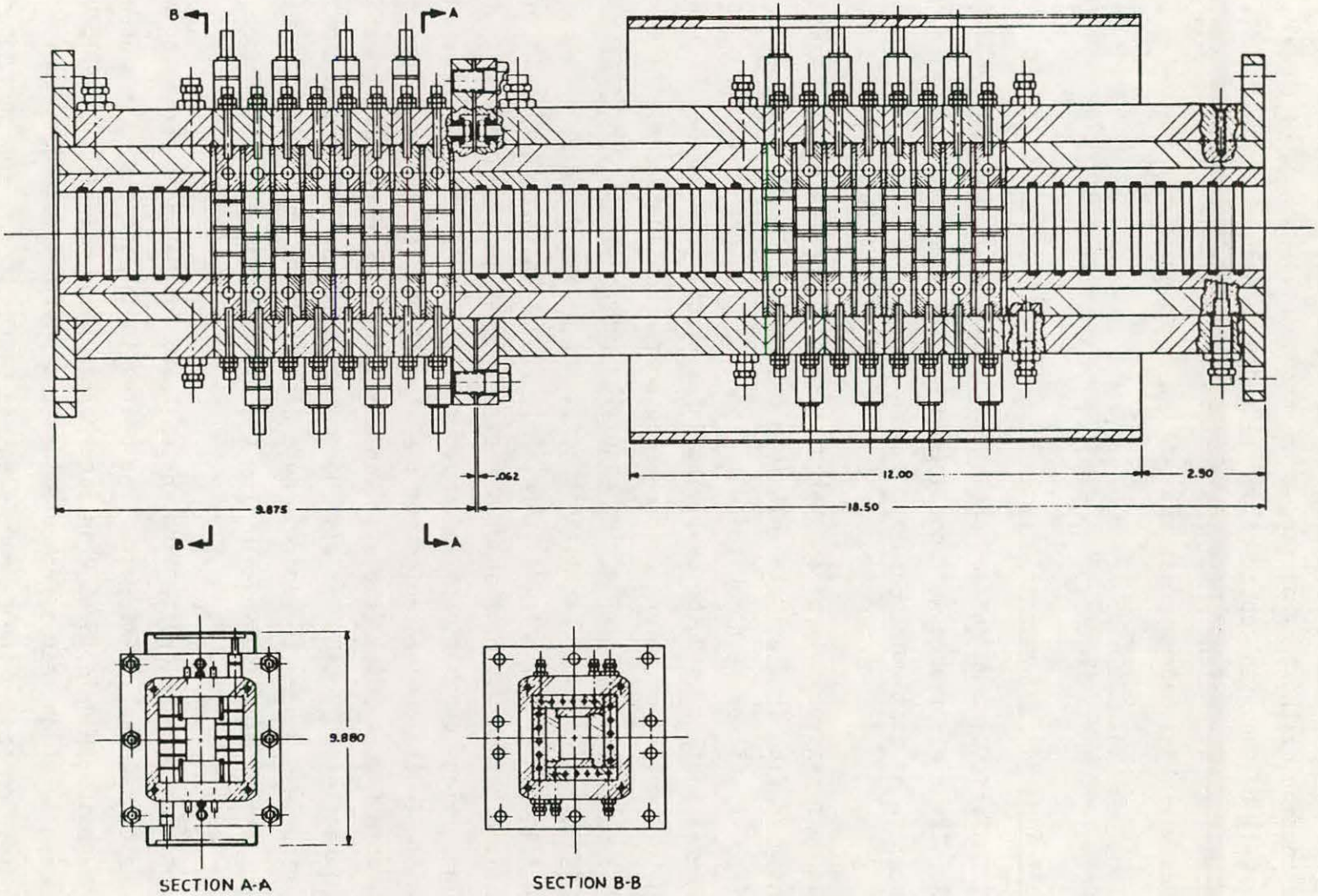

Figure 25. WESTF Test Section for WESTF Test 50

magnetic field and eight electrode pairs outside of the magnetic field in the entrance section of the test passage. The anodes will be made of copper; the cathodes will be tungsten-copper composite and/or copper. Sidewalls will be of a peg-wall construction. Plasma side insulation between pegs and between electrodes will be a magnesia castable backed-up by boron nitride.

2.1.3 Post-Test Analysis

WESTF Test 43

SEM-EDAX analysis was run on sections of the #5 anode and cathode from WESTF Test #43. These electrodes were considered to have undergone corrosion reactions representative of that which occurred in the channel.

The #5 anode consisted only of a layer of slag covering the nickel mesh. (Apparently, during the test, the platinum coated Al_2O_3 anode segments debonded from the nickel mesh substrate). The iron cathodes were highly corroded ($\approx$3 mm metal wastage) and the overlying thick slag layer was black in color compared to the thinner, brown colored slag coating on the anode. As shown in Figures 26(a) and 26(b), the electrode slag layers are complex mixtures of many components. Near the plasma interface, the glassy non-crystalline K_2O rich slags on both electrodes (Area 1 in Figure 26) are fairly similar except that the cathode slag is about six times richer in iron oxide than is the anode slag. Slag compositions, as computer calculated from EDAX data, are given in Table 8. In the cooler regions of the slag layers, Area 3 in Figure 26(a) and Area 4 in Figure 26(b) (see also Table 8), the glassy slag phase becomes completely depleted in CaO. It also becomes enriched in K_2O near the cathode and depleted in K_2O near the anode. Note also that the anode slag has picked up a large amount of dissolved NiO from the exposed "nickel mesh" anode.

The compositions of the crystalline phases found in the anode and cathode slag layers are considerably different. The phases in the anode slag are predominately nickel-magnesium-spinels (Spot 2 in Figure 26(b)) and metallic nickel particles (Spots 3 and 5) which result from chemical and physical degradation of the mesh. The principle phases in the cathode slag are magnesium and aluminum doped iron oxides (Spots 4 and 5 Figure 26(a)) and to a lesser extent magnesium-iron-spinels (Spot 2).

SLAG

PLASMA

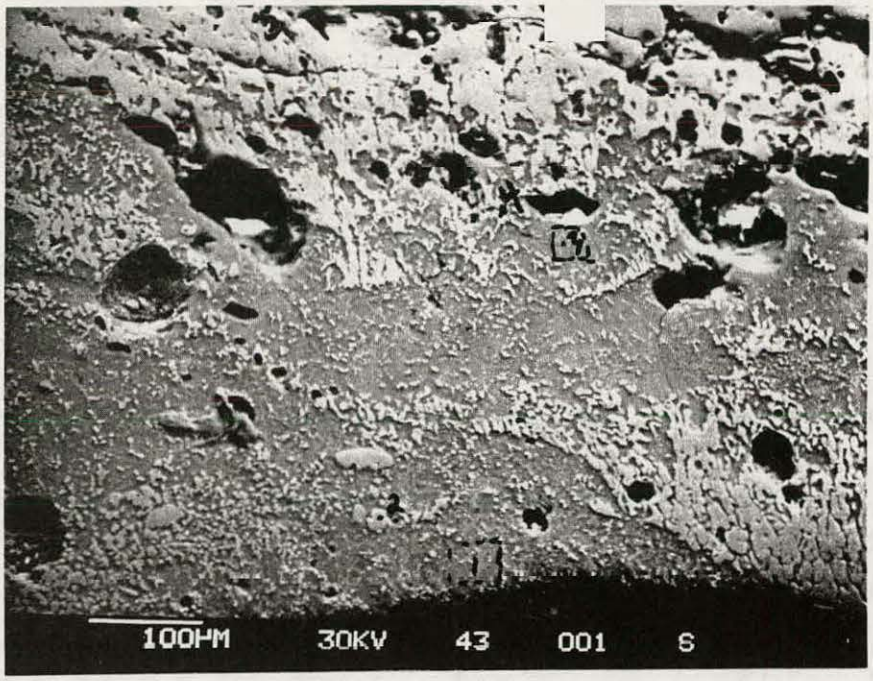

(A) Cathode

NICKEL

SLAG

PLASMA

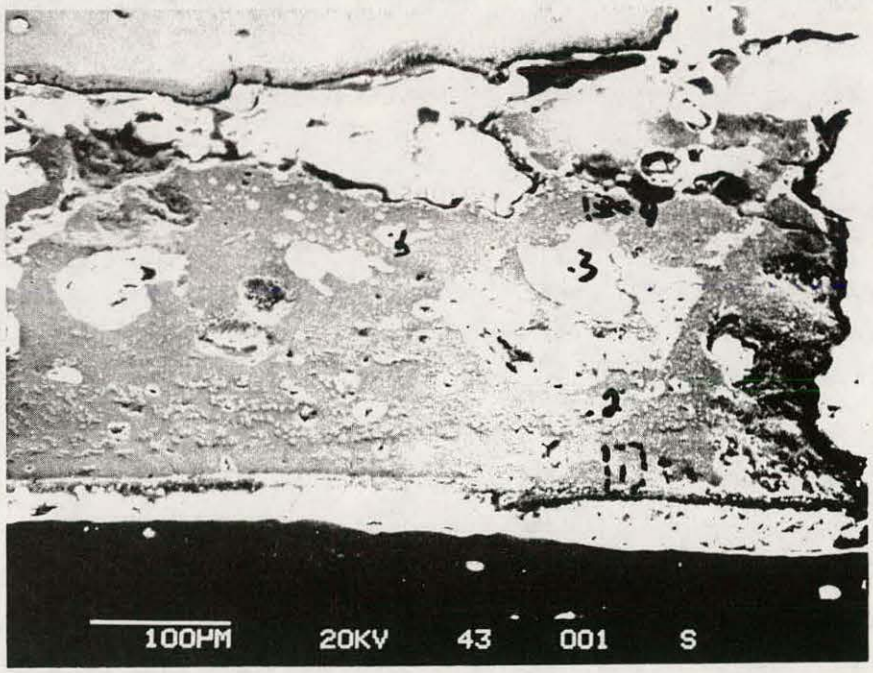

(B) Anode

Figure 26. SEM Photomicrographs of Slag Layers on (A) Cathode and (B) Anode from Electrode #5, WESTF Test #43

TABLE 8

CALCULATED SLAG COMPOSITIONS FROM WESTF TEST #43

LOCATION	SLAG COMPOSITION, W/O							
	SiO_2	Al_2O_3	FeO	CaO	MgO	TiO_2	NiO	K_2O
Area (1) Cathode (Figure 26 (a))	31.9	15.4	10.9	9.5	3.8	0.8	--	27.8
Area (1), Anode (Figure 26 (b))	38.4	16.7	1.8	11.3	3.7	0.5	--	27.6
Area (3), Cathode (Figure 26 (a))	36.2	18.5	10.1	--	2.4	--	--	32.9
Area (4), Anode (Figure 26 (b))	44.3	26.7	2.1	--	0.2	0.7	13.0	13.1

Figure 27 illustrates that the iron cathode has undergone grain-boundary corrosion (Spot 6), the reaction products being iron oxides. This result, coupled with the earlier observation that the cathode slag is very rich in iron oxides as well as the fact that no metallic iron was found in the slag, indicates that reducing conditions which would normally be expected at cathode walls in MHD channels were not obtained in this particular test.

There are two possible explanations as to why oxidizing conditions prevailed at the cathode wall. One is that the cathodes were not completely covered by slag during at least part of the test. Without a slag layer, electrochemical stresses, which give rise to reducing conditions, cannot be developed; thus, the iron cathodes were exposed to the relatively oxidizing conditions of the combustion plasma. The second explanation is that the electrical current was not transferred uniformally across the cathode slag layer during a large part of the test. This condition would arise if alternate current paths (i.e., leakage paths) existed that were less resistive than those through the slag layer. Although it is not presently possible to choose between the best above scenarios, it is clear that the extremely high corrosion rates of the iron electrodes in WESTF Test #42 resulted from an inability to maintain reducing conditions at the cathode wall.

WESTF Test 45

The SEM-EDAX test results on the ZrO_2-20 m/o Y_2O_3 cathode are in many ways similar to that reported earlier for the anode (Reference 3). However, liquid slag constituents have penetrated somewhat deeper into the cathode than at the anode (i.e., 0.90 mm versus 0.65 mm) and the concentration of K and Fe components in the slag were always greater than at the anode. The higher potassium content in the slag may explain why the cathode was more bloated and cracked than the anode. It was also found that both zirconium and ytrrium were more soluble in the cathode slag than in the anode slag.

In all regions of the electrode where slag has condensed, it is very highly enriched in calcium compared to the original composition of the Rosebud flyash used in these experiments. The general trend in slag composition as one traverses from the electrode surface toward the interior is increasing Al, Si and K content but decreasing Ca content. However, even in the interior of the electrode, the calcium concentration is still greater than in the original flyash.

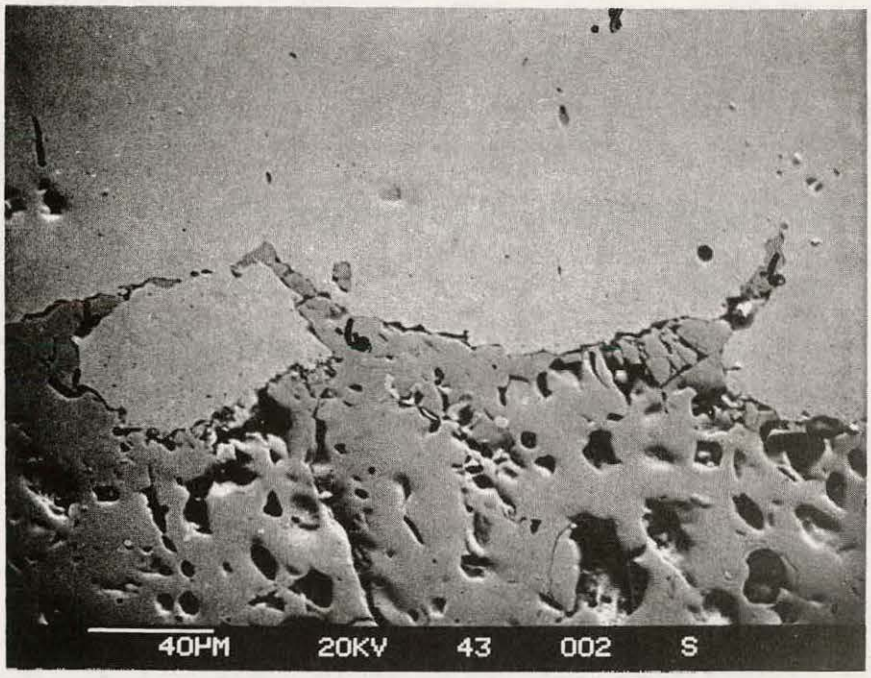

IRON
CATHODE

SLAG

Figure 27. SEM Photomicrograph of Grain Boundary Corrosion of Iron Cathode

As seen in Figure 28, the surface regions of the ZrO_2 (Y) anode, in addition to having experienced grain growth and spheroidization, has undergone changes in chemical composition. At the hotter regions, the ZrO_2 has picked up calcium from the slag while ytrrium and to a lesser extent the zirconium itself has dissolved into the slag. Although the ZrO_2 (Y) cathode had blackened somewhat at the platinum electrical leadout, no evidence for intermetallic Pt-Zr compounds could be found.

2.2 WBS 1.2.2 - Test Assembly Fabrication

During this quarter the following test section fabrication activities were completed or were in process:

- Completion of the dummy test section, an entrance section, and a downstream pipe section for the first flow train.
- Completion of a prototype WESTF II frame.
- Fabrication of all WESTF II test section components.

Fabrication activities on the MTS II test sections (cold and hot) and the MTS II viewport have been deferred until the latter part of the year as a result of a revision of test plans.

Dummy Test Section Flow Train

The Dummy Test Section (DTS) is the term given to a refractory lined, water-cooled, flanged steel pipe section that is used for facility checkout runs in place of the more sophisticated test section. It was remade to have a 1.96 in. x 1.41 in. flow area and mocked up to have the WESTF II envelope dimensions (9.88 in. x 5.25 in.) in the area where WESTF II would pass through the magnet. It will be used to (1) ensure proper fitup of WESTF components up to, through, and beyond the magnet and (2) to be used for facility checkout runs without the magnet.

The (DTS) flow train extends from the mixer flange (upstream) to the reducer flange (downstream). The overall length of the flow train is 52-5/8 $\pm$ 1/8 inches, and it consists of the components listed below:

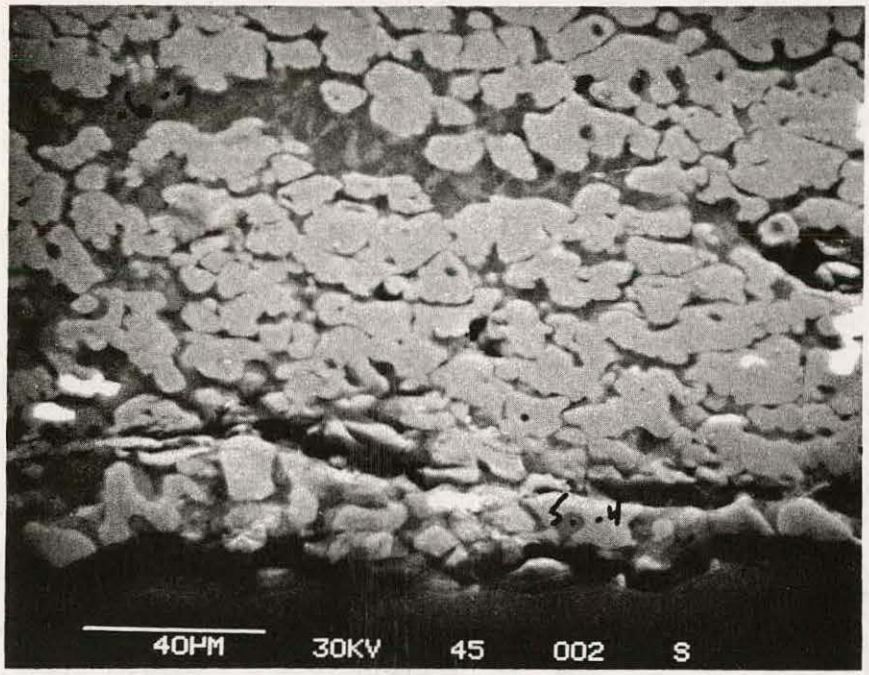

CATHODE

PLASMA

Figure 28. SEM Photomicrograph of Slag Intruded Surface Region of ZrO_2- 20 m/o Y_2O_3 Cathode - WESTF Test 45 (Darker Areas Surrounding Spheroidized ZrO_2(Y) Grains are Slag)

Mixer Flange/Copper Nozzle	Upstream
Gasket	.062
Entrance Section	9.875 ± .005
Gasket	.125
Dummy Test Section	20.000 ± .005
Gasket	.125
Spray Section	9.625
Gasket	.125
Downstream Pipe	12.500 ± .005
Gasket	.125
Reducer Flange	Downstream

The entrance section is the region of plasma flow stabilization in the transition from the mixer nozzle to the test components or, in this case, the DTS. The upstream flange on the entrance section is designed to envelope the extension of the copper nozzle through the mixer flange; the downstream flange bolts to the DTS. Both of these sections are lined with castable MgO to give a centrally located 1.41 in. x 1.96 in. flow passage inside the 4 in. diameter pipe and are externally water cooled. The DTS contains four 1/8-in. pipe couplings to be used for pressure taps, optical sight ports and thermocouples which are to be installed as required by the facility operating team. Aluminum side bars are attached by threaded fasteners to the corners of the extended plates to give an overall envelope dimension of 5.200 in. x 9.888 in., a dimensional constraint for all channels that will be tested in the magnet. Photographs of the entrance section and the DTS are given in Figure 29.

WESTF-II Test Section Components

A prototype WESTF II frame has been completely assembled and is shown in Figure 30. The frame width is 1.40 in. and contains two copper anodes, two W-Cu capped copper cathode and four insulating peg wall sub-assemblies. A cross section showing the internal details of the structure is shown in Figure 24. The electrode heat sinks are of a standard construction with copper plugs and stainless tubes silver soldered to the body. The ends of the stainless tubes are grit blasted to grip the flexible nylon water tubing more securely. Key components of the peg wall design are shown in Figure 31. G-11 plates electrically isolate the

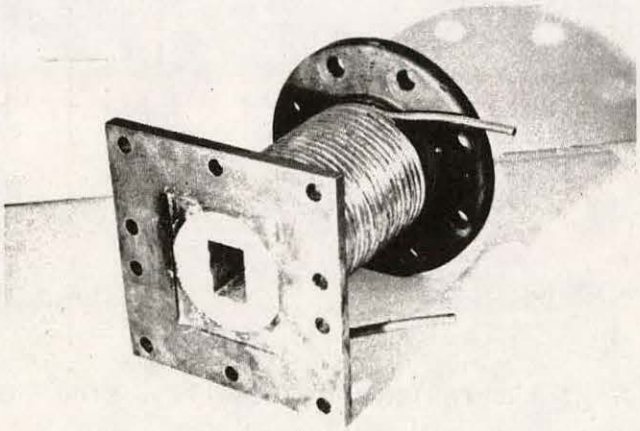

A) Entrance Section

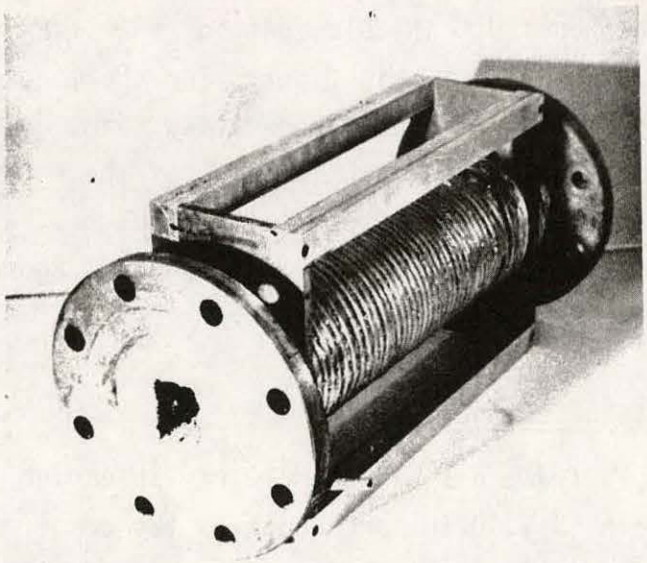

B) Dummy Test Section

Figure 29. Dummy Test Section Flow Train Components

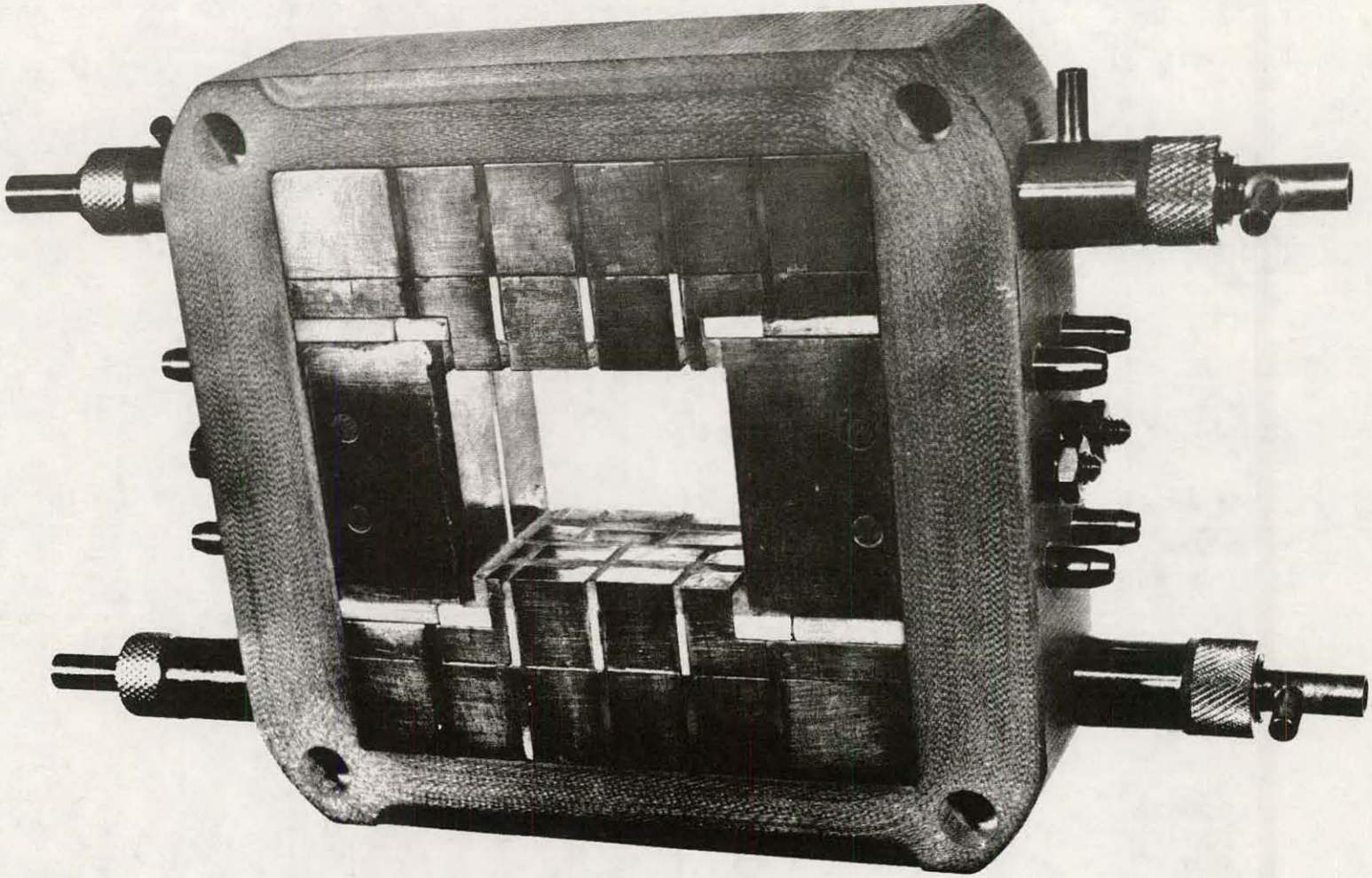

Figure 30. WESTF II Prototype Frame Assembly

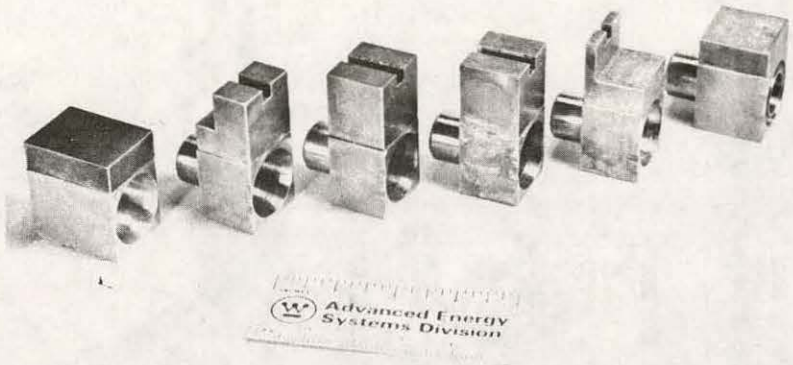

A) Peg Wall Cooling Blocks

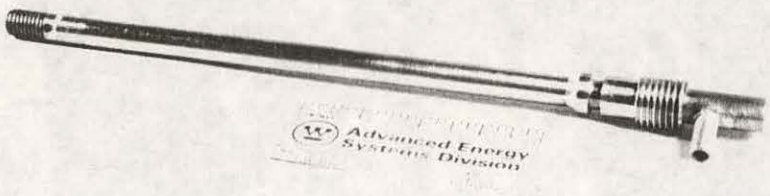

B) Cooling Tube Subassembly

C) Cooling Channel Extension

Figure 31. Key Components of WESTF II Peg Wall Assembly

blocks in the area of the water passage. "O" rings form the water seal. A nylon coating on the cooling channel extension electrically insulates between the inlet and outlet tubing. Either boron nitride or boron nitride and a castable ceramic form the insulation at the channel interface with slag.

Hydraulic tests on the various sub-assemblies showed them to be leak tight to at least 100 psig and to have cooling water flows that are adequate for the planned initial tests. Flow data will be recorded for each of the water circuits in the sub-assemblies going into a test assembly.

Mechanical tests were performed on one of the early frames (frame width 1.05 in.). Holes that had been drilled through the frame perpendicular to the channel axis were plugged with G-11 rod epoxied in place, and the frame was sealed between two metal plates using formed-in-place silicon rubber gasket material. After allowing a sufficient time for curing of the seals, the frame was internally pressurized. A pressure of 175 psig was reached before there was any evidence of a leak and this occurred at an epoxied plug. As the pressure was increased to 200 psig, leaks also developed at the gasket seal. These pressures are well in excess of the maximum design operating pressure of 75 psig.

An area of special concern is the web between the inside corners of the frame and the tie rod holes. An examination of this area of the frame after the internal pressurization showed no change. In order to obtain quantitative data a destructive test was run on a tensile testing machine. Figure 32 shows the samples on the test apparatus. First, a tensile load was applied to the frame as shown in Figure 32(a). Breaking began at a load of 775 pounds as a crack that initiated at a point where the natural laminations intesected with the top machined surface of the frame. Other cracks of that type followed until an ultimate load of 2140 pounds was reached. At this load, the frame broke at the top mid-open where some plugged holes were present. The bottom portion of the frame was cut into two "L" shaped specimens that were tested as shown in Figure 32(b). In this case, a bending moment was applied with a 0.5 inch diameter punch acting at a point located 2.5 in. from the vertical wall. In each case the first break was the extension of the cracks that were present from the tensile test. This occurred at a load of 265 pounds for the first sample and at 250 pounds for the second sample. The ultimate load was that at which the corner cracked and was 350 pounds for the first sample and 375 pounds for the second sample.

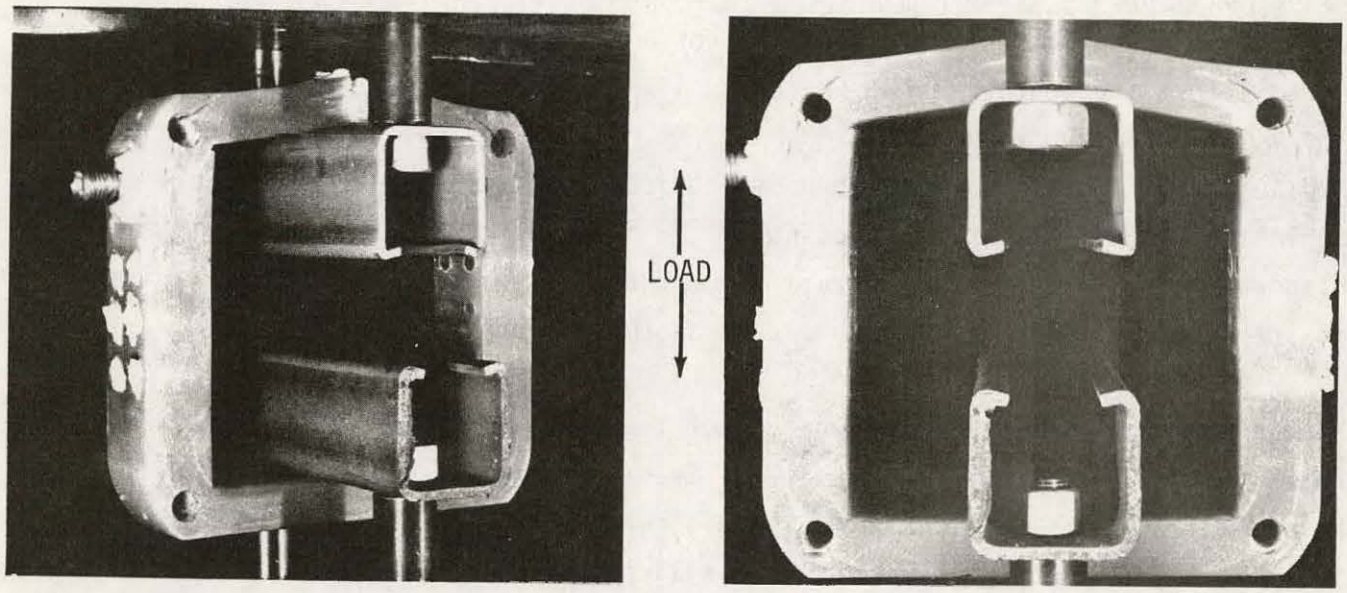

A) Tensile Test

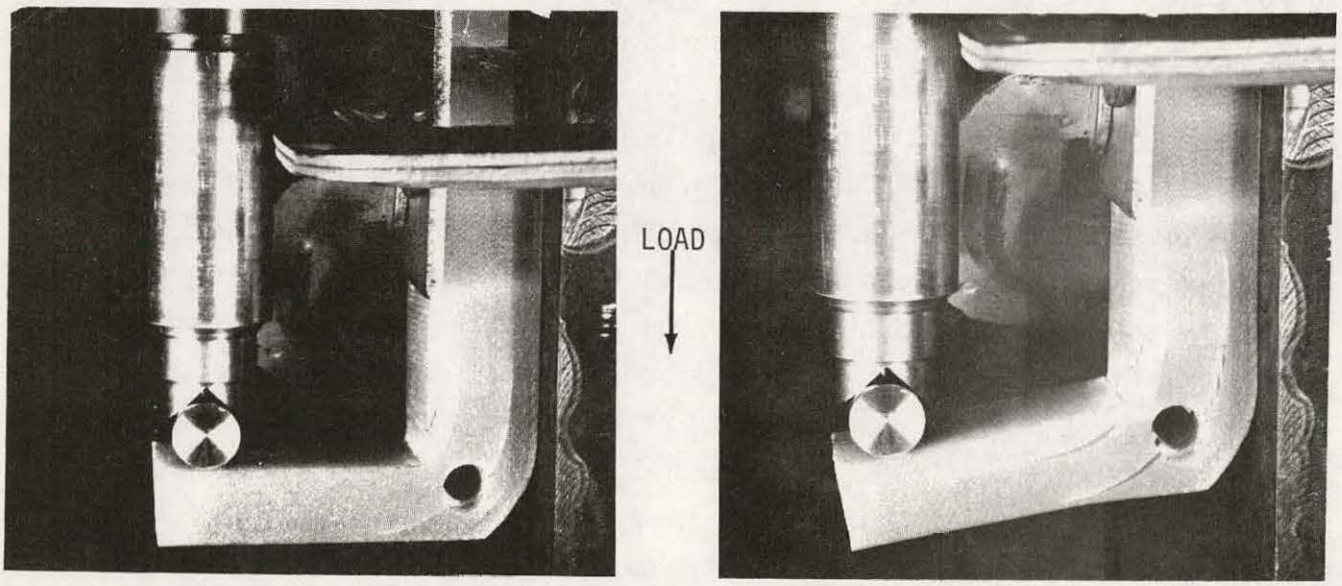

B) Bending Test

Figure 32. Mechanical Testing of G-11 Frame

Several attempts were made to fabricate tungsten-copper composite (Elkonite 10W 3) capped cathodes by vacuum brazing the cap to the copper heat sink without sources. Even though a vendor recommended cleaning procedure was used, the bond between the two materials lacked strength. Better bonding was obtained, however, by torch brazing with silver solder and a paste flux. The capped cathodes used in the first test sections will be made by this technique.

Samples, approximately .080 in. thick, of two grades of boron nitride (one a a moisture-resistant grade) were subjected to 97% relative humidity at 53°C for a total time of 216 hours. Weight changes were measured at several time intervals and are compared in the following table.

MOISTURE ABSORPTION OF BORON NITRIDE INSULATOR CANDIDATES

TIME OF EXPOSURE TO 97% R.H. AT 53°C (HOURS)	WEIGHT GAIN, %	
	GRADE A	GRADE H.P.
24	1.8	.41
96	3.0	.54
216	4.3	.58

These data show a considerable difference in the weight gains of the two materials. However, there was no visible or structural change in either sample. Therefore, it was concluded that the Grade A material is suitable for use in short duration tests, such as those to be run in the WESTF facility, at about one-half the cost of the Grade HP material.

The fabrication of all component parts for the initial cold WESTF II test has been essentially completed. Brazing and soldering of the various sub-assemblies required for the inlet, test, and outlet sections are in progress. Detailed assembly instructions have been prepaed for the electrode frame components. The preparation of assembly instructions for the inlet and outlet sections have been initiated.

2.3 WBS 1.2.3 - WESTF Operations

There has been no activity within this task during the reporting period due to the facility modification activity which is discussed below.

3.0 WBS 1.3 - WESTF MODIFICATIONS

3.1 MINI-COMPUTER/DAS

Upgrading of the mini-computer was completed during the prior quarter.

3.2 MAGNET INSTALLATION

Continued good progress has been achieved in most areas associated with the magnet modification, magnet installation and supporting facility modification activities.

The following summarizes significant accomplishments during this reporting period (further details are presented in succeeding paragraphs):

- The WESTF flow train has been completely disassembled and rework is in process.
- Magnet modifications, including electrical and hydraulic checkouts, have been completed.
- The magnet has been delivered to the R&D Center and positioned in the facility; the magnet control panel has been installed in the control room.
- The magnet power supply has been received and installed in the facility.
- The flow train hoist has been installed.
- Completion of installation of the 440V power transformer.

- Completion of hookup of the facility to the recirculating water system.
- Completion of fabrication of the water flow panel and new mixer nozzle.
- The Dummy Test Section, to be used for facility checkout following completion of facility modifications, has been fabricated and delivered.
- Installation of thermocouple and electrical patch panels, including wiring between the patch panel and the control room.
- Rewiring of electrical supply to the test section power supplies.
- Fabrication and installation of the load bank.

Overall views of the control room and test area are shown in Figures 33 and 34.

3.2.1 Magnet Modification

All primary modifications were completed during the prior quarter. Hydraulic and electrical checkouts were completed, as discussed below, and the magnet was delivered to the R&D Center and positioned within the facility.

Hydraulic Testing

According to the specification to which the magnet was rebuilt, the modified coils were to be leak tight when pressurized to 150 psi. The coils of the magnet were subject to hydraulic pressures in excess of 150 psi with no evidence of leaks. However, flow testing of the coils of the magnet indicated that the flows were inadequate in a number of the water flow circuits. In order to reduce overall water pressure requirements the coils had been originally designed so that the flow of water through the individual circuits of the magnet were in parallel while the electrical circuits were in series. The flow blockage noted was due to mineral deposits within the coil cooling channels which resulted from operation and storage of the magnet at Waltz Mills. Sulfonic acid, and warm dilute hydrochloric acid were pumped through the individual circuits of the

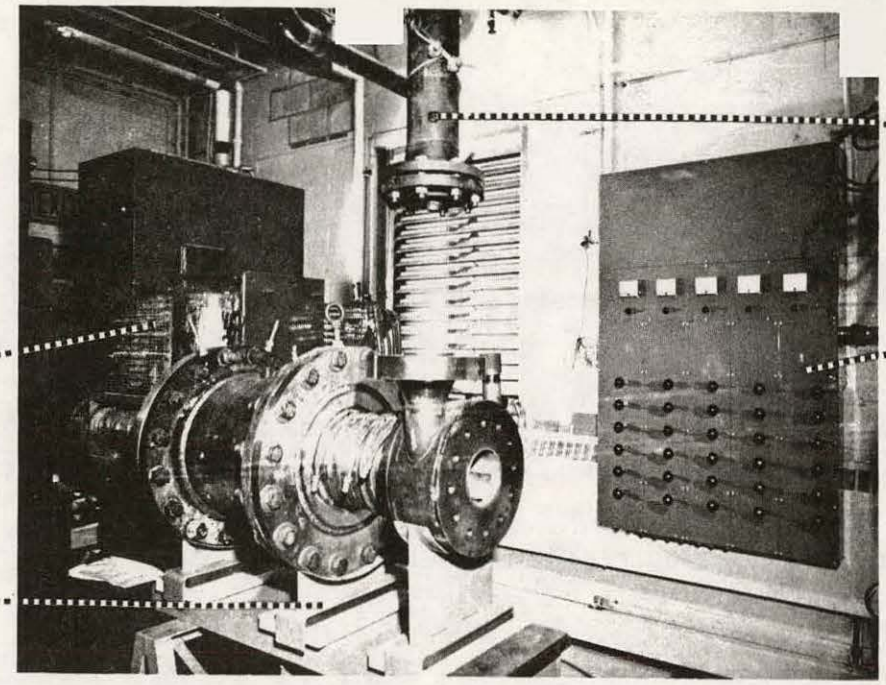

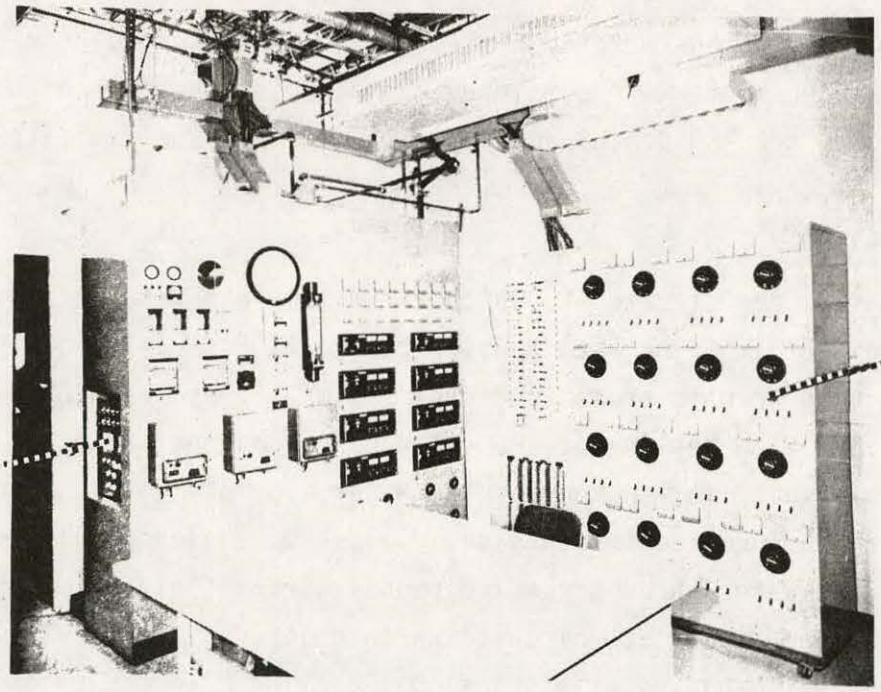

Figure 33. WESTF Status Photo

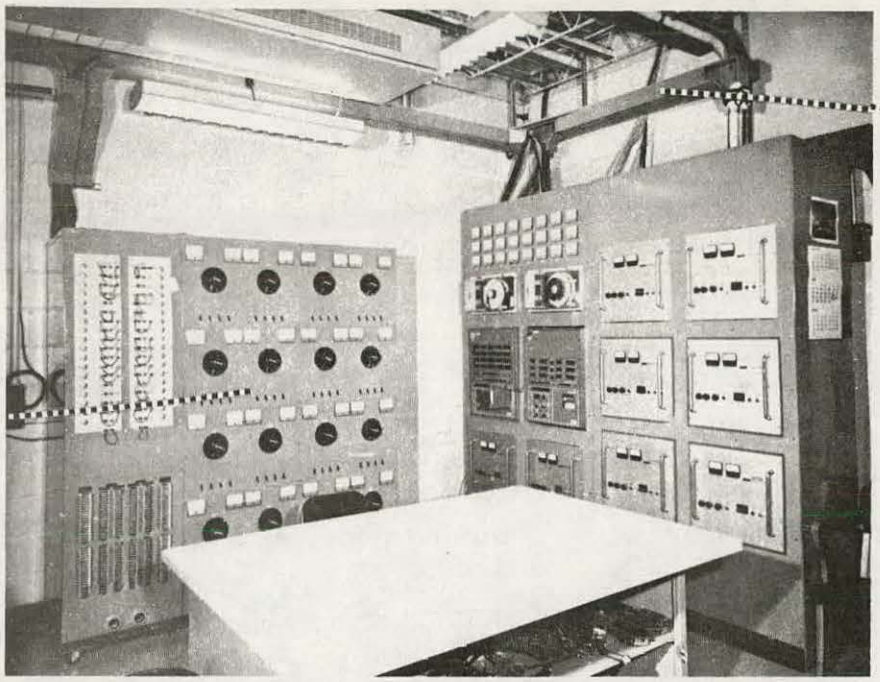

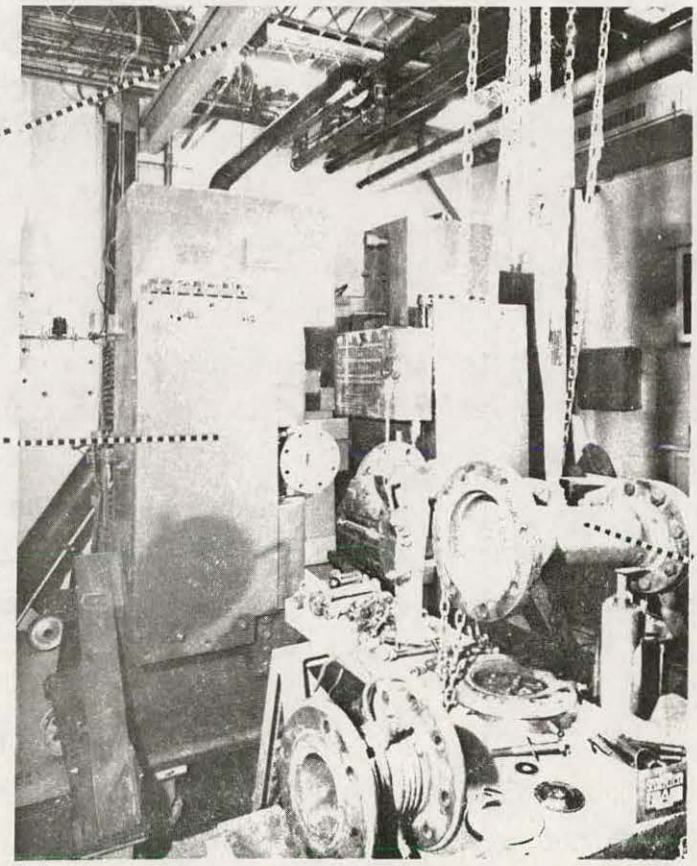

Figure 34. WESTF Status Photo

magnet at different times to remove the blockage. Use of these chemicals cleared the blockage in all but 2 or 3 of the 15 individual circuits of each coil. These water circuits were cleared of obstruction through the use of standard lye solutions. Upon completion of the cleaning operation each individual water circuit was capable of delivering better than .85 gal/min. at a ΔP of 85 psi. This flow is adequate.

Individual water flow metering will be mounted in the circuit of each coil during installation of the magnet in WESTF to monitor if further deposits are accumulating during operation so that corrective action can be taken. The water going to the magnet is filtered to further reduce the chance of blockage.

Electrical Testing

Following a Vapor Pressure Impregnation of the two overall coil assemblies under vacuum with a special insulating resin, the specified series of electrical tests were performed on the completely assembled magnet. First, 3000 volts DC was applied between the coils and the core section of the magnet and the voltage held for one minute. The power supply voltage was then reversed and the test repeated. There was no evidence of breakdown and the insulation resistance was greater than 4000 megohms.

The resistance of each individual 20 turn coil was measured on both halves of the magnet. The resistances showed from 17×10^{-3} ohms for the longer coils to 9×15^{-3} ohms for the shorter coils. The variation in coil resistance with position of the two halves of the magnet were almost indentical.

The turn-to-turn insulation of the magnet was checked using P-J instrumentation. In this test a frequency of about 7700 cycles per second was applied to each half of the magnet and voltage brought to 2800 volts, corresponding to 10 volts per turn. There was no evidence of any breakdown.

The anticipated operating voltage of each half of the magnet at the 1200 ampere maximum loading is about 225 volts. A 600 volts RMS AC voltage was applied to each half of the magnet, and the voltage drop across each individual coil measured. The current drawn for each side of the magnet was about 18 amperes.

The variation in voltage with position across the individual coils of both halves of the magnet were identical under this condition.

In the last electrical test a 1200 volts RMS AC voltage was applied across each half of magnet. A current of about 31 amperes was drawn. The volt amps across the individual coils were again measured. Again the variation in voltage drop across the individual coils was identical for both halves of the magnet. The above tests clearly showed that the magnet insulation to ground, the turn-to-turn insulation, and voltage drop in normal operation are acceptable.

3.2.2 General Modifications

In parallel with the basic modification associated with installation of the magnet it was decided to implement a number of facility design and hardware changes. The primary additions to the basic modification include the following:

- Fabrication of a recirculating water system flow control panel.
- Inclusion of a trench and T/C, electrical and water system patch panels.
- Revamping of the seed system.
- Redefinition of the flow passage geometry, from 1 in. x 2 in. to 1.43 x 1.96 in. (bare dimensions) as discussed in Section IV-2.1.2.
- Extensive rewiring of the control room, including new electrical and instrumentation wiring from the test area to the control room.

These modifications will greatly expand the flexibility of the modified facility.

Flow Panel

Fabrication of the flow panel was completed and the unit delivered to the WESTF facility. It consists of 30 water circuits, 12 of which are rated at 12-120 GHP and 18 of which are rated at 30-300 GHP. The flow through each of these circuits is monitored by a turbine flow transducer that interfaces with an electronic module. The electronic module contains an integral power supply that drives a light emitting diode (LED) in the transducer and the circuitry required to pick

up a signal from the LED and condition it to provide a 0-5 volt analog output for input into the WESTF computer.

Flow can be calibrated and controlled by adjusting any of the six 1/2 inch valves, twelve 3/8 inch valves, or twelve 1/4 inch valves located on the front of the panel. Above each band of six valves are a selector switch and a GPH calibrated voltmeter that can be used to establihsed the desired flow rates for each circuit at the panel location. Once the flow are established and a run is in progress, flow monitoring will be done remotely by the computer.

Insulating Section of Preheated Air Line

The design of an insulating length of piping for the WESTF an preheater was described in Reference 3. All of the component parts of this section have been fabricated. Assembly in preparation for installation in WESTF is in process.

4.0 WBS 1.4 - PROJECT MANAGEMENT AND DOCUMENTATION

The following required project documentation was issued during the reporting period:

- Monthly Report for March 1980
- Monthly Report for April 1980
- Monthly Report for May 1980
- Quarterly Report for January-March 1980

A number of discussions were held with DOE personnel to further focus the direction of and plans for future contract activities. In support of this effort, visits and contacts with AVCO Everett Research Laboratory were continued to review their current activities.

V. SUMMARY PLANS NEXT REPORTING PERIOD

Summary plans covering significant activities during the next reporting period, July-September 1980, are presented below according to the Work Breakdown Structure primary tasks.

WBS 1.1 - ELECTRODE AND INSULATOR MATERIALS

- Based on the literature search, define a list of materials as potential candidates to replace platinum as an anode cladding material.
- Continue development and evaluation of test methodology associated with the anode arc erosion test.
- Initiate the evaluation of electrochemical corrosion tests for screening cold metallic electrode materials.
- Continue development of attachment techniques for ceramic materials to be tested in WESTF in upcoming tests.

WBS 1.2 - ENGINEERING TESTS

- Finalize Work Plan which is directed towards the engineering development and evaluation of slagging cold metallic electrodes.
- Issue Test Specifications applicable to WESTF Tests 50 through 53.
- Complete assembly of the test section for WESTF Test 50.
- Initiate fabrication activities in support of WESTF Test 51 and 52.
- Complete facility safety review.
- Complete facility checkout operations.

WBS 1.3 - WESTF MODIFICATIONS

- Complete modifications associated with installation of magnet.

WBS 1.4 - PROJECT MANAGEMENT AND DOCUMENTATION

- Issue monthly status reports.
- Issue April-June 1980 Quarterly Report.
- Issue Project Management Summary Baseline Report covering FY 81.
- Participate in project review meeting with cognizant DOE personnel.

VI. CONCLUSIONS

Considerable progress has been achieved in completing modifications associated with the addition of the conventional 3 Tesla magnet to WESTF. All major procurement actions have been completed and the equipment items have been positioned within the facility. A significant amount of effort remains to be done, particularly in completing electrical, instrumentation and hydraulic interconnections. The facility flow train hardware has been modified and is in process of being reinstalled. Post-modification subsystem checkouts will be completed next quarter. It is projected that initial system operation with a dummy test section will be completed by the end of the next quarter.

Continued progress has been made in refining the test methodology applicable to the laboratory anode arc test. A number of further improvements have been identified to improve the discrimination and reliability of this laboratory screening test.

The recently completed literature search has provided a sound base for selecting potential materials which could be alternatives to platinum for use on anode electrodes. Although the atmosphere at the anode is not quantitatively known, it is probable that it is a highly oxidizing and SO_3 rich environment similar to that which occurs when coal is burned in an oxygen rich atmosphere, i.e., a hot corrosion atmosphere such as found in gas turbines and fireside coal atmospheres. The highly oxidizing environment is electrochemically generated. It is clear that anode alloy selection criteria should be based on its being refractory and on its having a refractory protective scale.

VII. REFERENCES

1. FE-15529-2, "MHD Electrode Development, Quarterly Report, January - March 1979," DOE Contract DE-AC-01-79-ET-15529, Westinghouse Electric Corporation, May 1979.

2. FE-15529-3, "MHD Electrode Development, Quarterly Report, April-June 1979," DOE Contract DE-AC-01-79-ET-15529, Westinghouse Electric Corporation, August 1979.

3. FE-15529-6, "MHD Electrode Development, Quarterly Report, January-March 1980," DOE Contract DE-AC-01-79-ET-15529, Westinghouse Electric Corporation, February 1980.

4. FE-15529-1, "MHD Electrode Development, Quarterly Report, October-December 1978,"DOE Contract DE-AC-01-79-ET-15529, Westinghouse Electric Corporation, January 1979.

5. R. Singh and K. Natesan, Corrosion-NACE, Vol. 36, 1980, p. 321.

6. V. J. Hruby, et.al., 7th International Conference on MHD Power Generation, MIT, June 1980.

7. L. H. Cadoff, et.al., Proceedings of 18th Symposium on Engineering Aspects of MHD, Butte, Montana, June 1979.

8. Open Cycle MHD Power Generation, Ed. by J. Heywood and G. Womack, Pergamon Press, 1969.

9. T. Hunary, et.al., J. of Metals, March 1979, p. 28.

10. K. Chiang, et.al., Conf. Corrosion/Erosion of Coal Corrosion System Mat'ls., Berkeley, California January 1979.

11. J. A. Goebel and F. S. Pettit, p. 693-710 in Metal-Slag-Gas Reactions and Processes, Ed. by Z. A. Foroulis and W. W. Smeltzer, The Electrochemical Society, Princeton, N.J., 1975.

12. C. Sims and W. Hagel, Eds., "The Superalloys," 1972 John Wiley and Sons.

13. J. Stringer, p. 14 in Proceedings Corrosion/Erosion of Coal Conversion Systems Mat'ls. Conf., Berkeley, California January 1979.

14. J. Stringer, p. 589 in "Ash Deposits and Corrosion Due to Impurities in Combustion Gases," Ed. R. W. Bryers, Hemisphere Publ. Corp., 1978.

15. J. Stringer, pp. 513-556 in Properties of High Temperature Alloys, Ed. by Z. A. Foroulis and F. S. Pettit, The Electrochemical Society, Princeton, N.J., 1975.

16. J. Stringer, Ann Rev. of Mater. Sci., Vol. 7, 1977, p. 477.

17. J. Stringer, p. K-95, in 4th Annual Conf. on Mat'ls. for Coal Conversion and Utilization, NBS, Oct. 1979.

18. J. Stringer, p. 331 in Proc. 1st Conf. on Advanced Mat'ls. for Alternative Fuel Capable Directly Fired Heat Engines," Castine, Me. July 1979.

19. R. Perkins, p. 351 in Proceeding Corrosion/Erosion of Coal Conversion Systems Mat'ls. Conf., Berkeley, California January 1979.

20. W. Apblett, p. 330 in Conf. Corrosion/Erosion of Coal Corrosion System Mat'ls., Berkeley, California January 1979.

21. J. Stringer and D. Whittle, p. 665 in Metal-Slag-Gas Reactions and Processes, Ed. Z. Foroulis and W. Smeltzer, The Electrochemical Society, 1975.

22. C. Corti et.al., Platinum Metal Rev., Vol. 24, 1980, p. 2.

23. J. L. Bates, "Evaluation of Platinum-Coated Copper Anode AVCO Mark VII", PNL, Richland, Washington, supported by DOE under Contract EY-76-C-06-1830.

24. R. D. Johnson, and B. H. Faulkenberry, Northrop Space Laboratories, Hawthorne, California, Diffusion Coefficients of Copper and Platinum into Copper Platinum Alloys, AFML, Wright-Patterson Air Force Base, Ohio, Contract No. AF 33(657)-8765, Project No. 7351, Tech. Report No. ASD-TDR-63-625, 1963.

25. R. E. Ogilvie, S. R. Moll, and D. M. Koffman, Advanced Metals Reserach Corp., Somerville, Mass., Research to Determine Composition of Dispersed Phases in Refractory Metal Alloys, Part II. Concentartions Gradients in Refractory Metal Binary Diffusion Couples, AFML, Wright-Patterson Air Force Base. Ohio, Contract No. AF 33(616)-7671, Project No. 7351, Tech. Report No. ASD-TDR-62-7, 1963.

26. Mathematical Tables Project "Table of Probability Function . . ", Vol. 1, Federal Works Administration, New York, 1941.

27. V. J. Hruby, et.al., "Electrode Development at AVCO Everett Research Laboratory, Inc.", Seventh International Conference on MHD Electrical Power Generation, Cambridge, MA, 1980.

☆U.S. GOVERNMENT PRINTING OFFICE: 1980-740-145/810